AUCTORES
Globalize your Research

International Journal of BioMed Research
Loutfy H. Madkour*

Open Access

Review article

Pharmacogenomics-Synergistic Strategies Using a Chimerical Peptide for Enhanced Chemotherapy Based on ROS and DNA Nanosystem

Loutfy H. Madkour

Chemistry Department, Faculty of Science Tanta University, 31527, Tanta, Egypt

Corresponding Author: Loutfy H. Madkour, Chemistry Department, Faculty of Science Tanta University, 31527, Tanta, Egypt

Received date: August 03, 2021; **Accepted date:** September 15, 2021; **Published date:** January 08, 2022

Citation: Loutfy H. Madkour (2022). Pharmacogenomics-synergistic strategies using a chimerical peptide for enhanced chemotherapy based on ROS and DNA nanosystem. *International J. of Biomed Research*. 2(2): DOI: 10.31579/IJBR-2021/035

Abstract

Co-delivery of gene and drug for synergistic therapy has provided a promising strategy to cure devastating diseases. The use of genomic predictors of response to cisplatin and pemetrexed can be incorporated into strategies to optimize therapy for advanced solid tumors.

Here, a positive feedback strategy was utilized to amplify the concentration of intracellular reactive oxygen species (ROS) and a ROS-triggered self-accelerating drug release nanosystem (defined as T/D@RSMSNs) was demonstrated for enhanced tumor chemotherapy. It was found that in human breast cancer (MCF-7) cells, T/D@RSMSNs could not only release DOX and a-TOS initiatively, but also lead to increased concentration of intracellular ROS, which could be used as new trigger to cut away TK linkage and then in turn facilitate the further release of DOX for enhanced chemotherapy. Standard treatment for advanced non–small-cell lung cancer (NSCLC) includes the use of a platinum-based chemotherapy regimen. This novel ROS triggered self-accelerating drug release nanosystem with remarkably improved therapeutic effects could provide a general strategy to branch out the applications of existing ROS-responsive drug delivery systems (DDSs).

Keywords: peptide; positive feedback strategy; ROS-responsive; tumor therapy; mesoporous

silica nanoparticle; drug delivery; synergistic therapy; p53; DOX

Here, an amphiphilic chimeric peptide $(Fmoc)_2KH_7$-TAT with pH-responsibility for gene and drug delivery was designed and fabricated. As a drug carrier, the micelles self-assembled from the peptide exhibited a much faster doxorubicin (DOX) release rate at pH 5.0 than that at pH 7.4. As a nonviral gene vector, $(Fmoc)_2KH_7$-TAT peptide could satisfactorily mediate transfection of pGL-3 reporter plasmid with or without the existence of serum in both 293T and HeLa cell-lines. Besides, the endosome escape capability of peptide/DNA complexes was investigated by confocal laser scanning microscopy (CLSM). To evaluate the co-delivery efficiency and the synergistic anti-tumor effect of gene and drug, p53 plasmid and DOX were simultaneously loaded in the peptide micelles to form micelleplexes during the self-assembly of the peptide. Cellular uptake and intracellular delivery of gene and drug were studied by CLSM and flow cytometry respectively. And p53 protein expression was determined via Western blot analysis. The *in vitro* cytotoxicity and *in vivo* tumor inhibition effect were also studied. The results [1] suggest that the co-delivery of gene and drug from peptide micelles resulted in effective cell growth inhibition *in vitro* and significant tumor growth restraining *in vivo*. The chimeric peptide-based gene and drug codelivery system will find great potential for tumor therapy.

The mesoporous silica nanoparticles (MSNs) based nanocarriers were gated by β-cyclodextrin (β-CD) through the ROS-cleavable thioketal (TK) linker to encapsulate the anticancer drug doxorubicin hydrochloride (DOX) and ROS producing agent α-tocopheryl succinate (α-TOS), whose surface was further anchored with adamantane conjugated poly(-ethylene glycol) chain (AD-PEG) via host-guest interaction. Both *in vitro* and *in vivo* experiments demonstrated that T/D@RSMSNs exhibited more significant antitumor activity in the human breast cancer than the traditional single-DOX loaded ROS-responsive nanocarrier.

1 Chemotherapy as synergistic gene

Chemotherapy as a dominant approach for the treatment of tumors has been widely used in clinical trials [2, 3]. However, the curative effect of chemotherapy is severely dampened due to severe systemic toxicity, low bioavailability of anti-tumor drug as well as the emerging of drug resistance of tumor cells after repeated administration of anti-tumor drug [4]. Gene therapy, which focuses on the modulation and repair of particular gene defect, provides a new avenue for tumor therapy in gene level. Unfortunately, the biosecurity concerns of viral vectors and the low transfection efficiency of non-viral vector greatly limit its application. Recently, synergistic therapy based on co-administration of gene and drug has emerged rapidly as a promising modality for tumor treatment. Decreased drug dosage, negligible side effect and high inhibition efficacy

are hopeful to achieve, mostly because of the synergistic effect [5] or reversal of drug resistance to some extent via specific gene [6] by the co-delivery systems.

The key point of synergistic therapy was to transport gene and drug to the same cells and tissues. Considerable efforts have been devoted to developing delivery systems and various carriers based on dendrimers [7], liposomes [8], polymers [9, 10] and nano-scaled inorganic particles [11] were proposed. But the barriers such as unsatisfactory cellular uptake, endosome escape and vectorinduced toxicity [12] are still fatal problems for these delivery systems. Especially in gene delivery process, the major DNA-loaded complex internalized into cells through endocytosis is believed to traffic from endosome to lysosome. The milieu in lysosome is hostile to DNA due to the existence of various enzyme systems, which may lead to the degradation of DNA/vector and failure in gene transfection [13]. Strategies based on the proton-sponge hypothesis are widely used to overcome the endosome escape barrier [14]. Generally, carriers with satisfied buffering ability always accompany with severe cytotoxicity, such as PEI and chloroquine.

Amphiphilic peptide-based micelles with a typical coreeshell structure are an important class of promising co-delivery systems for gene and drug [15, 16]. The peptide-based hydrophobic core can be used to encapsulate hydrophobic drugs, while the cationic peptide shells can be utilized to condense DNA. Additionally, benefiting from the blossom of modern molecular biology, peptides with tremendously appealing bioactivity have been exploited. For instance, TAT peptide (YGRKKRRQRRR), which derives from the transactivating transcriptional activator protein of HIV-1, has been confirmed to possess ability of autonomous and receptor independent cell membrane translocation [17, 18]. Besides, many viruses utilized pH-sensitive peptide to accelerate the endosome escape [19], pH-sensitive peptides such as GALA or histidine-rich peptide [20, 21] were fabricated as promising candidates to overcome the endosome escape barrier. Since peptide is originated from organism and mainly composed of nature amino acids, peptidebased biomaterials can always perform undeniable biocompatibility and biodegradability.

In this chapter, we reported an amphiphilic chimeric peptide, $(Fmoc)_2KH_7$-TAT with the chemical structure indicated in Scheme. 1, which can self-assemble into micelleplex with DNA and drug simultaneously.

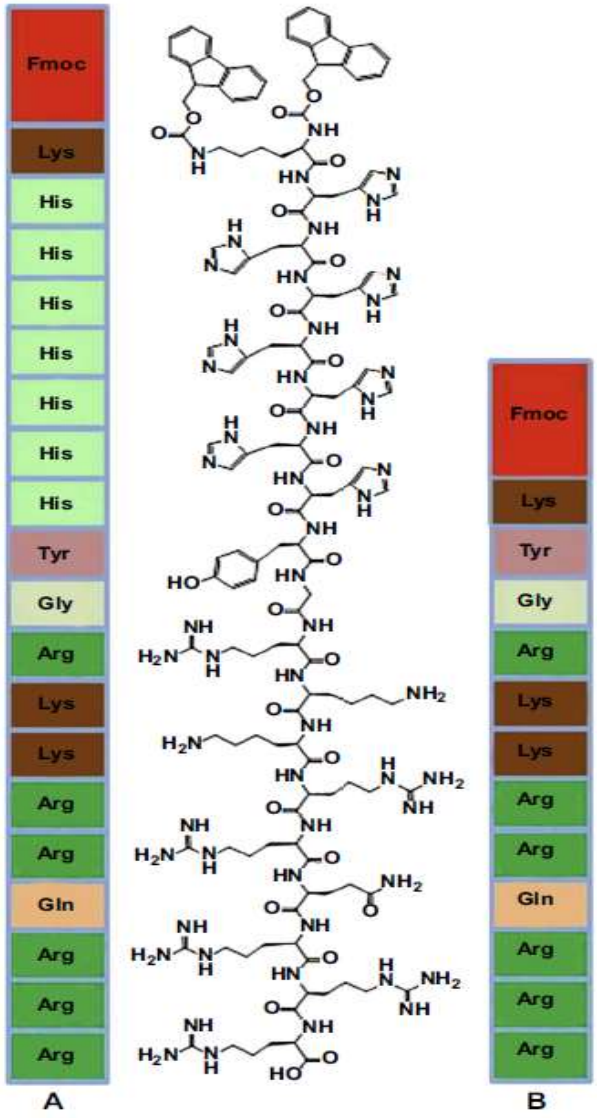

Scheme. 1 *The chemical structure of peptide: (A) (Fmoc)2KH7-TAT; (B) (Fmoc)2K-TAT.*

As illustrated in Scheme. 2, at the physiological pH, the hydrophobic drug DOX was encapsulated in the hydrophobic micellar core through hydrophobic interaction and π-π stacking interaction, while the DNAwas combined with cationic shell of TAT peptide. After cell internalization, the complexes could escape from the endosome due to the protonation of heptahistidine domain of $(Fmoc)_2KH_7$-TAT at low pH milieu, resulting in the swelling of complexes, accelerated drug release, and the delivery of therapeutic gene to nucleus subsequently. The properties of peptide micelles were characterized in terms of drug/DNA loading ability, drug release behavior in vitro, gene transfection ability as well as codelivery of gene/drug etc. Furthermore, the synergistic anti-tumor effect both in vitro and in vivo was evaluated in detail [1]

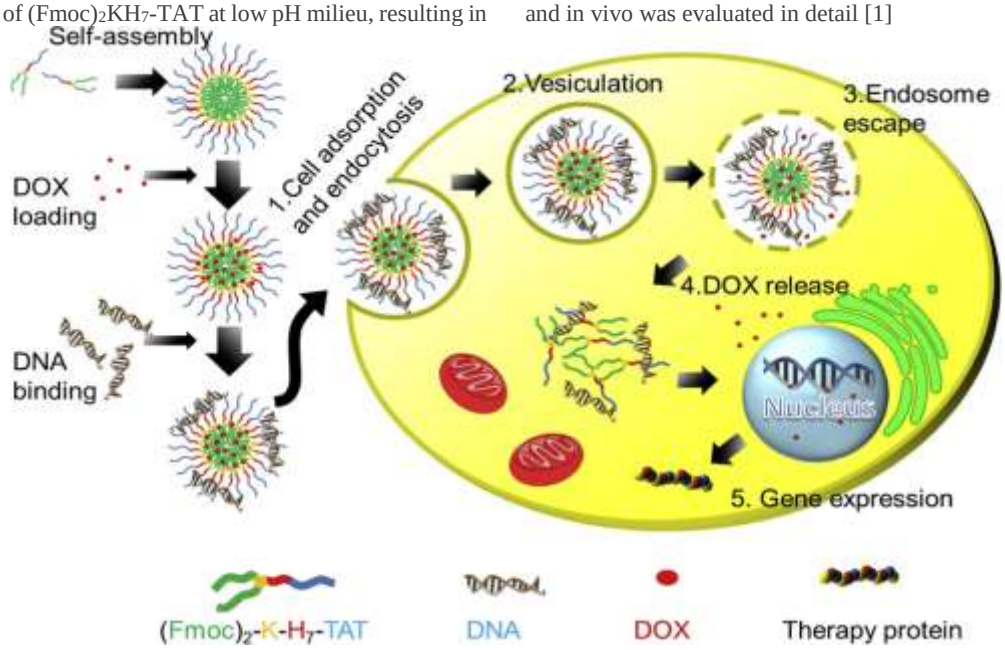

Scheme. 2 *Co-delivery and synergistic therapy of gene and drug by (Fmoc)2KH7-TAT micelleplex. (1) Endocytosis of DOX and gene loaded (Fmoc)2KH7-TAT, (2) vesiculation of the complexes, (3) endosome escape, (4) drug release and gene was delivery to nucleus and expression, (5) expression of therapy gene.*

2 Characterization of peptide and complexes

The condensation of DNA is crucial for gene transfection. To demonstrate the DNA binding ability of the micelles, agarose gel electrophoresis assay was studied. As shown in Fig. 1, $(Fmoc)_2KH_7$-TAT could completely retard the mobility of pGL-3 DNA at w/w of 5. The good DNA binding ability of $(Fmoc)_2KH_7$-TAT was probably due to the formation of micelle structure, since the DNA binding ability of TAT alone was relatively poor according to our previous work [22].

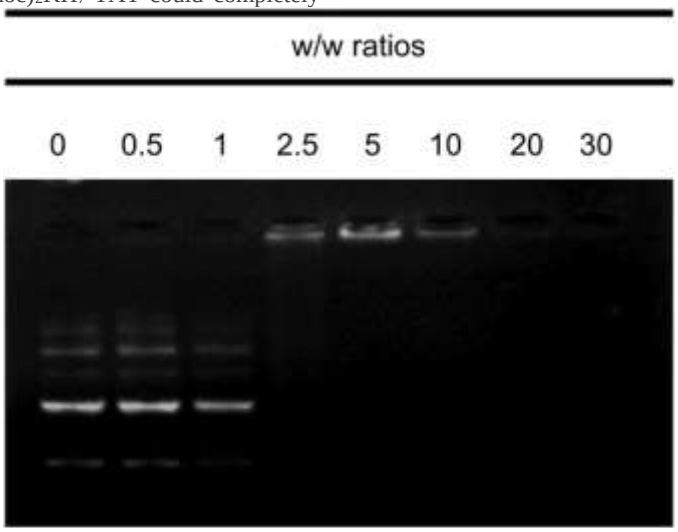

Fig. 1 *Agarose gel electrophoresis retardation assay of (Fmoc)2KH7-TAT/pGL-3 DNA complexes at various w/w ratios.*

Besides, the particle size and zeta potential of $(Fmoc)_2KH_7$-TAT/pGL-3 DNA complexes were also determined as shown in Fig. 2. The size decreased and the zeta potential increased with increasing w/w ratio, indicating the more compact complexes formed. Furthermore, size and zeta potential of DOX/ (Fmoc)2KH7-TAT/pGL-3 DNA micelleplexes were performed to investigate the influence of loaded drug. It was found that loading of DOX brought nearly negligible influence in zeta potential, while the loaded DOX increased the size slightly as compared with that of the $(Fmoc)_2KH_7$-TAT/pGL-3 DNA complexes, indicating that the loaded DOX swelled the micellar hydrophobic core to some extent.

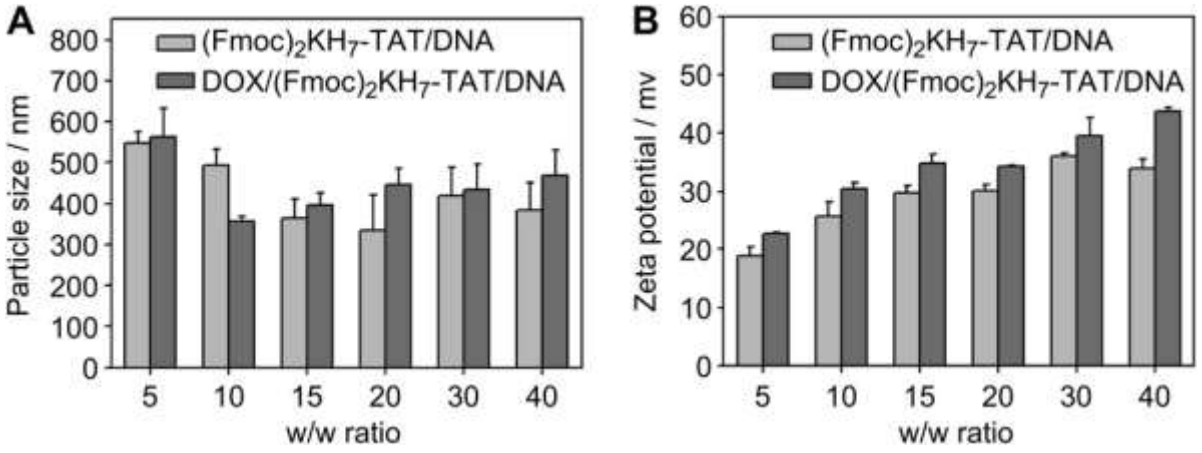

Fig.2. *Size (average diameter) and zeta potential of (Fmoc)2KH7-TAT/pGL-3 DNA complexes and DOX/(Fmoc)2KH7-TAT/pGL-3 DNA micelleplexes at various w/w ratios. Data are presented as mean ± S.D. (n = 3).*

In order to get direct insight into fabricated $(Fmoc)_2KH_7$-TAT micelles, and evaluate the effect of DNA and/or drug loading on peptide micelle, four corresponding morphologies were observed by TEM. As shown in Fig. 3A2-D2, all the samples were welldispersed with uniform structure. The loaded DOX increased the size of both peptide and peptide/pGL-3 DNA complexes. No matter drug was loaded or not, the condensation of DNA decreased the size of peptide micelles. The decreased size in complexes was attributed to the introducing of electrostatic interaction between cationic peptide and DNA. Furthermore, the hydrodynamic size of the four types of nanoparticles at the same peptide concentration was studied by dynamic light scattering (DLS). As shown in Fig. 3A1-D1, the tendency in hydrodynamic size was consistent with the TEM results. Moreover, the size observed by TEM was smaller than that by DLS and the discrepancy was ascribed to the shrinking of complexes during the preparation of TEM samples [23].

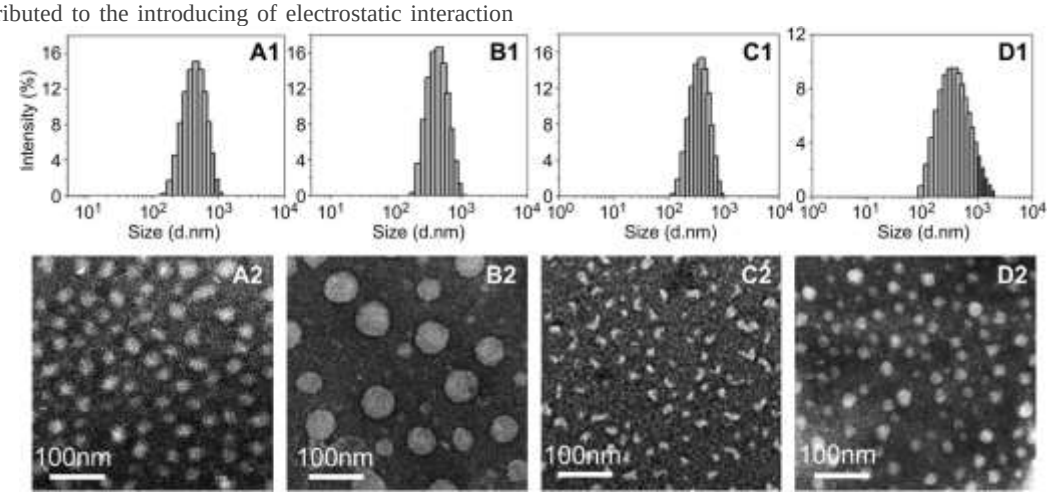

Fig. 3 *TEM images of (A) (Fmoc)2KH7-TAT; (B) drug loaded (Fmoc)2KH7-TAT; (C) (Fmoc)2KH7-TAT/pGL-3 DNA complexes; (D) DOX/(Fmoc)2KH7-TAT/pGL-3 DNA micelleplexes. The w/w ratio of peptide/pGL-3 DNA complexes was 15, and the observation was under PBS buffer (pH 7.4, 5 mM).*

3 Drug loading and release behavior in vitro

DOX was chosen [1] as the model drug to assess the drug loading behavior, and the EE and DLE values of peptide micelles were 21.8% and 11% respectively at pH 7.4. The peptide could efficiently entrap the DOX due to the π-π stacking interaction between Fmoc group and DOX as well as hydrophobic interaction between deprotonated histidine and DOX at neutral pH. To demonstrate the endosome-pH sensitivity of $(Fmoc)_2KH_7$-TAT, the drug release behaviors under different pHs were also evaluated, and pH 5.0 was chosen to imitate the endosome pH. As reflected in Fig. 4, the cumulative release of DOX at pH 5.0 was significantly faster than that at pH 7.4. This finding was attributed to the increased hydrophilicity of the peptide at pH 5.0. Since the pKa of imidazole group of histidine was about 6.0, the protonation of imidazole under slightly acid environment would vanish and destroy the hydrophobic interaction between H_7 and DOX, leading to the decrease in compactness of micelles and rapid release of drugs at pH 5.0.

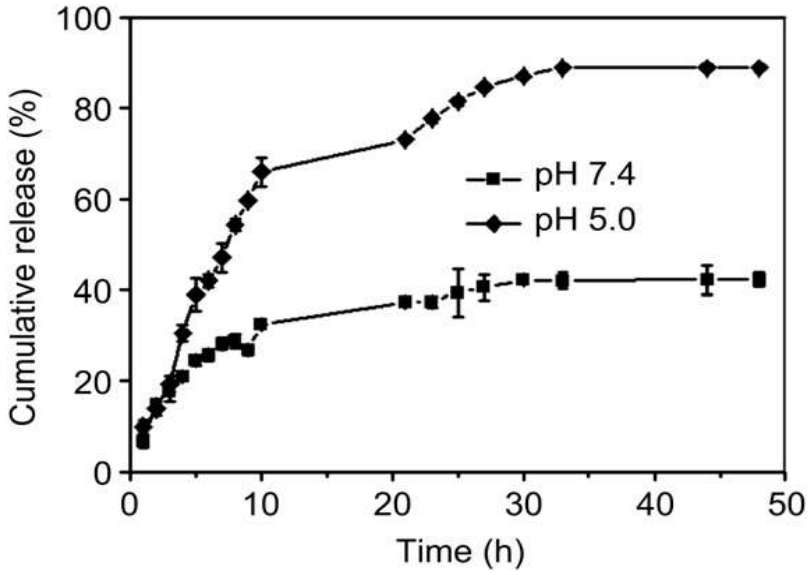

Fig. 4 *In vitro drug release behavior of DOX-loaded (Fmoc)2KH7-TAT micelles at different pHs (pH 7.4 and 5.0). Data are presented as mean ± S.D. (n = 3).*

4 Endosome escape capability

Translocating through plasma membrane mediated by TAT peptide was confirmed involving the classical endocytosis-uptake pathway [14]. As a result, complexes are always trafficked into endosome vesicles. Successfully conquering the endosome barrier is vital to co-delivery delivery system. Here, CLSM observation was performed to estimate the endosome escaping ability of $(Fmoc)_2KH_7$-TAT/pGL-3 DNA complexes. The complexes were labeled with FITC,while LysosomeRedwas specially used to stain the acidic organelles lysosome. $(Fmoc)_2K$-TAT/pGL-3 DNA was used as a negative control, and the corresponding ESI-MS of $(Fmoc)_2K$-TATwas studied [1]. As shown in Fig. 5, only a small amount of $(Fmoc)_2KH_7$-TAT/pGL-3 DNA complexes was trapped in lysosome, and the majority of complexes escaped from the endosome successfully, which was confirmed by the isolated distribution of red fluorescence and green fluorescence in Fig. 5D2. In contrast, the existence of large area of yellow fluorescence in Fig. 5D1 suggested that the majority of $(Fmoc)_2K$-TAT/pGL-3 DNA complexes was localized in lysosome.

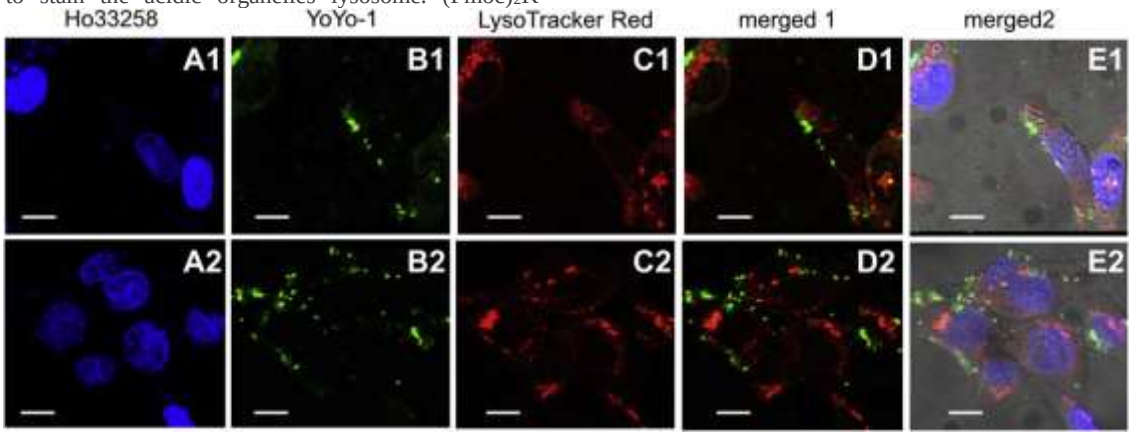

Fig. 5 *Endosome escape of (Fmoc)2KH7-TAT/pGL-3 DNA complexes (A1eE1) at w/w ratio of 15, (Fmoc)2K-TAT/pGL-3 DNA complexes (A2eE2) was used as a negative control. (A1, A2) Nucleus was stained with Hoechst 33258 (blue signal); (B1, B2) pGL3-DNA was labeled with YOYO-1 (green signal); (C1, C2) DOX (red signal); (D1) an overlay of (B1) and (C1); (D2) an overlay of (B2) and (C2). The scale bar was 10 mm and the micrographs were obtained at a magnification of 600x.*

5 Gene transfection in vitro

The luciferase expression of pGL-3 DNA mediated by $(Fmoc)_2KH_7$-TAT was investigated in 293T and Hela cell-lines. Herein, branched 25 kDa PEI was used as a positive control. Fig. 6A1 and B1 revealed that $(Fmoc)_2KH_7$-TAT performed comparable transfection efficiency to 25 kDa PEI at an optimal w/w ratio of 1.3 in both cell-lines under serum-free condition. Results demonstrated that the peptide could mediate satisfactory gene transfection. The multifunctional peptide with low cytotoxicity could form micelles through self-assembly which could enhance the stability of the complexes greatly. Moreover, excellent cellular uptake and endosome escape ability of the complexes could extremely improve their bioavailability.

The transfection ability under 5% serum-containing condition was further assessed as shown in Fig. 6A2 and B2. Due to the negative influence of serum to cationic gene carrier, the transfection efficiency mediated by PEI or $(Fmoc)_2KH_7$-TAT decreased to some extent in both cell-lines. However, the transfection efficiency of peptide was still comparable to that of 25 kDa PEI.

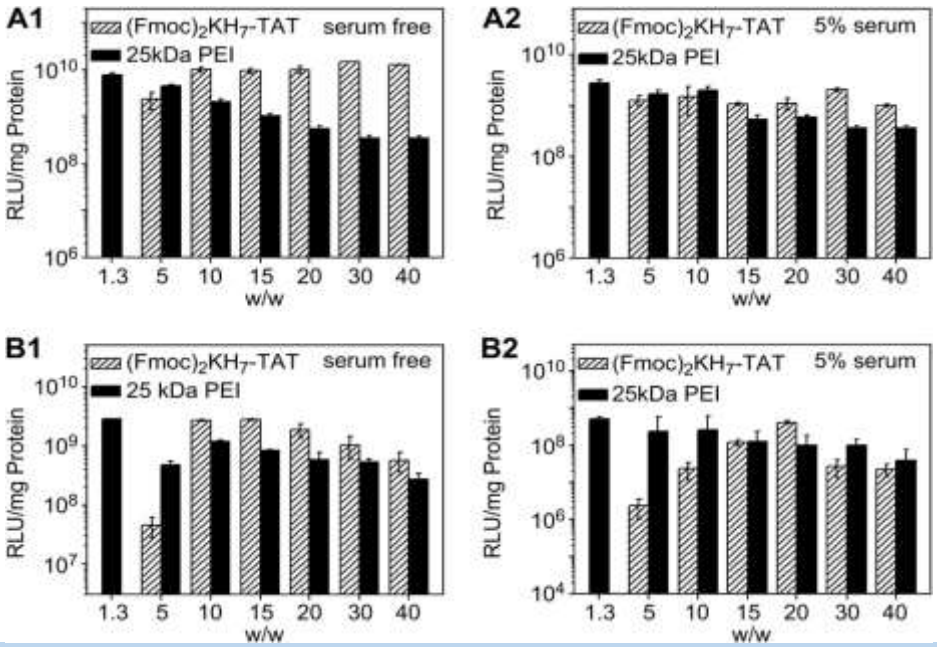

Fig. 6 *In vitro luciferase expression of (Fmoc)2KH7-TAT/pGL-3 DNA complexes at various w/w ratios in (A) 293T and (B) HeLa cell lines. 25 kDa PEI was employed as a positive control. Data are presented as mean ± S.D. (n = 3).*

6 In vitro cytotoxicity

As a good gene carrier, low cytotoxicity of vector itself was essential for practical applications. Cytotoxicity of $(Fmoc)_2KH_7$-TAT in vitro was estimated against HeLa cells via MTT assay. 25 kDa PEI was used as a negative control. As shown in Fig. 7A, the cell viability was still above 90% when the concentration of peptidewas 250 mg/L. On the contrary, the PEI showed serious cytotoxicity. Obviously, the peptide presented negligible toxicity, originating from the inherent biocompatibility of peptide.

The toxicity of doxorubicin hydrochloride (DOX.HCl) and DOX loaded peptide system is also shown in Fig. 7B. The IC_{50} (the concentration required for 50% inhibition of cellular growth) of free DOX was 0.17 mg/L, while the one of DOX encapsulated in peptide micelles was 1.45 mg/L. Since the peptide was biocompatibility, the cytotoxicity was mainly induced by the release of loaded DOX. It was also found that at low DOX concentration, free DOX showed significantly higher cytotoxicity than DOX loaded peptide. With the increasing concentration of DOX, the difference in cytotoxicity between them was decreased, since free DOX can be readily transported into cytoplasm and nuclei by passive diffusion, while the DOX release from micelles was time-consuming [24].

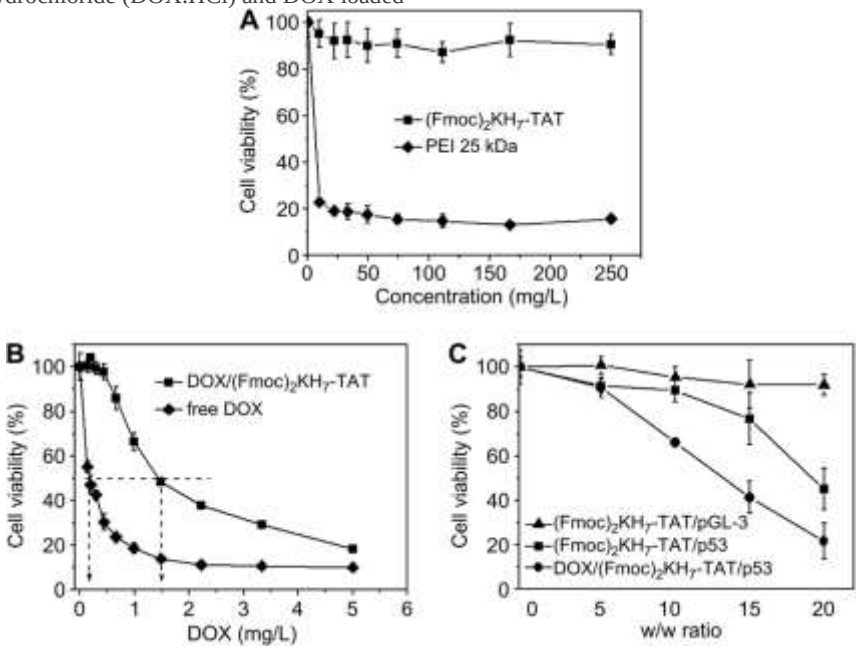

Fig. 7 *In vitro cytotoxicity against HeLa cells: (A) (Fmoc)2KH7-TAT and 25 kDa branched PEI; (B) free DOX and DOX loaded (Fmoc)2KH7-TAT; (C) (Fmoc)2KH7-TAT/pGL-3 DNA complexes, (Fmoc)2KH7-TAT/p53 DNA complexes and DOX/(Fmoc)2KH7-TAT/p53 DNA micelleplexes with the DOX concentration of 0.5 mg/L.*

7 Co-delivery of drug and gene in vitro

In HeLa cells, the nucleus was stained with Hoechst 33258 (blue) and pGL-3 DNA was labeled with YOYO-1 (green). The w/w ratio of (Fmoc)2KH7-TAT/pGL-3 DNA was 15, while the final concentration of DOX was 0.638 mg/L because the toxicity at this concentration was negligible. Cellular uptake at different time (1 h and 4 h) was performed as shown in Fig. 8. With the increasing incubation time, the green and red fluorescence intensity increased significantly, indicating that the uptake of micelleplexes was time-dependent. Besides, the green and red fluorescence got well overlapped after internalization for 4 h (Fig. 8D2). In the light of this finding, peptide micelles could successfully load pGL-3 DNA and DOX simultaneously. The excellent co-delivery behavior may benefit from the core-shell structure of the cationic peptide micelles. Meanwhile, image of merged2 at 4 h revealed that the majority of DOX/peptide/pGL-3 DNA micelleplexes entered the nucleus or were around the nucleus periphery (Fig. 8E2).

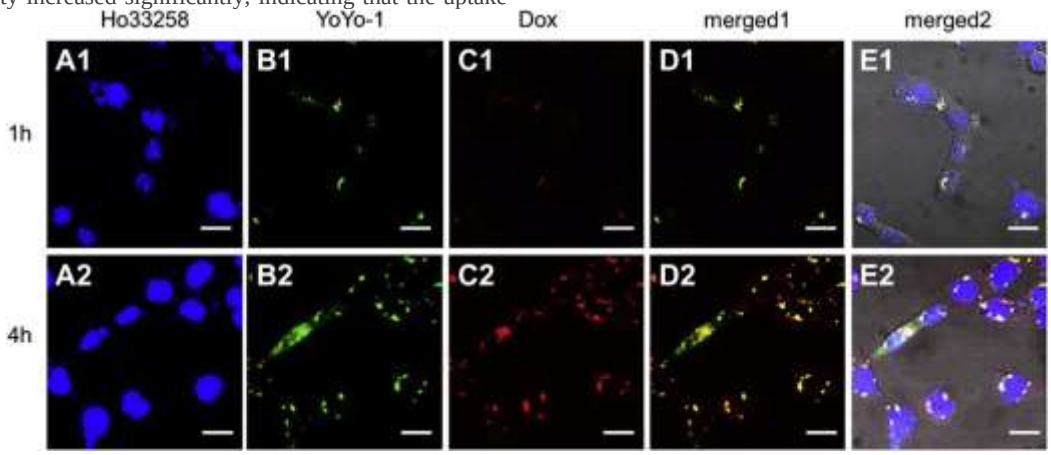

Fig. 8 *Co-delivery of drug and gene into HeLa cells via (Fmoc)2KH7-TAT with different time (1 h and 4 h) by CLSM, the w/w of peptide/pGL-3 DNA complexes was 15 and the final concentration of DOX was 0.638 mg/L. (A1, A2) Nucleus was stained with Hoechst 33258 (blue signal); (B1, B2) pGL3-DNA was labeled with YOYO-1 (green signal); (C1, C2) lysosome was stained with LysoTracker Red DND-99 (red signal); (D1) an overlay of (B1) and (C1); (D2) an overlay of (B2) and (C2). The scale bar was 15 μm and the micrographs were obtained at a magnification of 600x.*

To further quantify the simultaneous delivery of gene and drug, two-color flow cytometry was performed as shown in Fig. 9. The $(Fmoc)_2KH_7$-TAT micelle was used as a blank control. Here, YOYO-1 stained $(Fmoc)_2KH_7$-TAT/pGL-3 DNA complexes were green fluorescence positive and DOX loaded $(Fmoc)_2KH_7$-TAT were red fluorescence positive. As expected, double-positive cells presented an overwhelming majority of the cells. This result demonstrated the excellent ability of the peptide in co-delivery of DNA and DOX to the same cells.

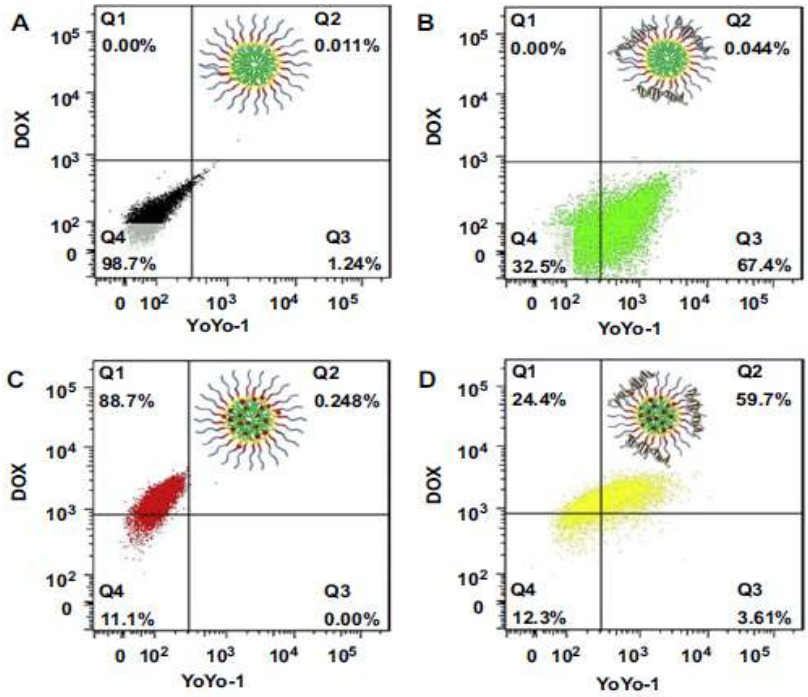

Fig. 9 *Co-delivery of gene and drug mediated by (Fmoc)2KH7-TAT by two-color flow cytometry in HeLa cells. The w/w of peptide/pGL-3 DNA complexes was 15 and the final concentration of DOX was 0.638 mg/L. (A) (Fmoc)2KH7-TAT was used as a negative control; (B) YOYO-1 stained peptide/pGL-3 DNA complexes was green fluorescence positive; (C) DOX loaded peptide was red fluorescence positive; (D) YOYO-1 stained DOX/peptide/pGL-3 DNA micelleplexes*

8 Synergistic effects *in vitro*

The key point of co-administration of gene and drug was to achieve synergistic effect. Herein, the cell viability against HeLa cells via MTT assay was employed to evaluate the synergistic effect in vitro. p53 gene was chosen as a therapy gene to suppress the growth of tumor. As shown in the Fig. 22.7C, $(Fmoc)_2KH_7$-TAT/pGL-3 DNA exhibited negligible toxicity in HeLa cells, while $(Fmoc)_2KH_7$-

TAT/p53 DNA complexes showed certain cytotoxicity. The DOX/$(Fmoc)_2KH_7$-TAT/p53 DNA micelleplexes presented significantly higher cytotoxicity than that of $(Fmoc)_2KH_7$-TAT/p53 DNA complexes. Since the concentration of loaded DOX in micelleplexes was 0.5 mg/L, the loaded DOX showed negligible cytotoxicity according to Fig. 7B, the much increased cytotoxicity was attributed to the synergistic effect of DOX and p53 gene. Clearly, co-administration of gene and drug exceedingly decreased the dose of DOX in peptide micelles and resulted in the enhanced cell growth inhibition rate.

To further confirm the synergistic effect, Western blot analysis was used to determine the p53 protein expression in different transfected cells. GAPDH was used as the internal control. According to Fig. 10A, peptide induced very low expression level of p53 protein. Additionally, $(Fmoc)_2KH_7$-TAT/p53 DNA could mediate higher expression level of p53 protein than that of 25 kDa PEI/p53 DNA (*w*/*w* 1.3), demonstrating the excellent gene transfection efficacy of $(Fmoc)_2KH_7$-TAT in vitro once again. Remarkably, DOX/(Fmoc)2KH7-TAT/p53 micelleplexes mediated considerably higher expression level of p53 protein than either $(Fmoc)_2KH_7$-TAT/p53 DNA complexes or DOX loaded $(Fmoc)_2KH_7$-TAT. This result was consistent with that in cytotoxicity. Besides, the relative p53 protein expression was also provided in Fig. 10B. The relative p53 protein expression was assessed as the light intensity ratio of p53 to GAPDH from Western blot results in Fig. 10A.

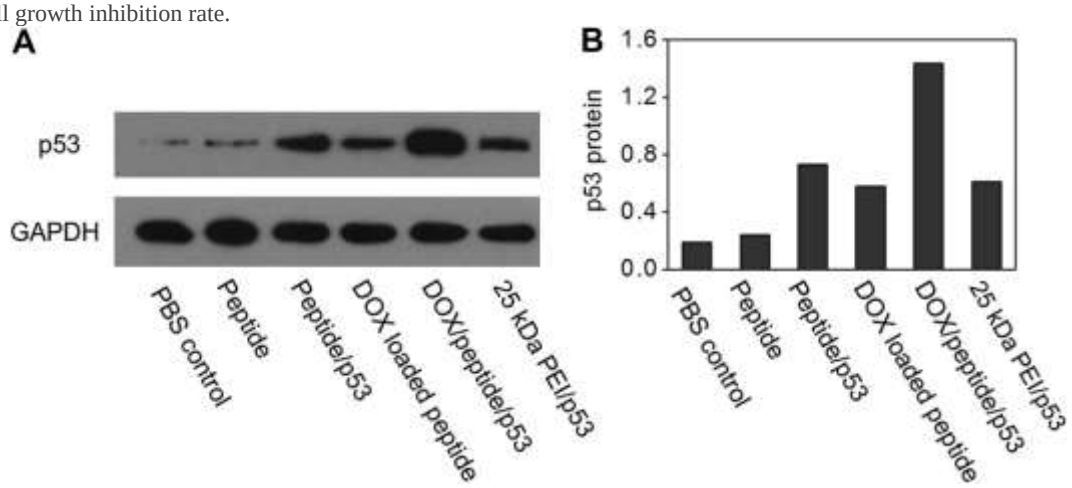

Fig. 10 *(A) p53 protein expression determined via Western blot analysis; (B) analysis of light intensities of p53 protein expression as the ratio of p53 to GAPDH from Western blot results, GAPDH was used as an internal control.*

9 Anti-tumor effects *in vivo*

The anti-tumor effect in vivo of PEI/p53 complexes, DOX loaded $(Fmoc)_2KH_7$-TAT, $(Fmoc)_2KH_7$-TAT/p53 DNA complexes and Dox/$(Fmoc)_2$KH7-TAT/p53 DNA micelleplexes was tested, and PBS was used as the control. Fig. 11 revealed that all testing groups showed certain anti-tumor effect compared to PBS control. In detail, $(Fmoc)_2KH_7$-TAT/p53 DNA complexes exhibited better tumor inhibition than 25 kDa PEI/p53 DNA complexes, indicating the superiority of $(Fmoc)_2KH_7$-TAT in gene delivery in vivo. Notably, DOX/$(Fmoc)_2KH_7$-TAT/p53 DNA micelleplexes performed remarkably higher efficiency in tumor inhibition than either $(Fmoc)_2KH_7$-TAT/p53 DNA or DOX loaded $(Fmoc)_2KH_7$-TAT, attributed to the synergistic effect of co-delivery of gene and drug. Similar results were also found from the tumor separated from mice at the 11th day after treatment.

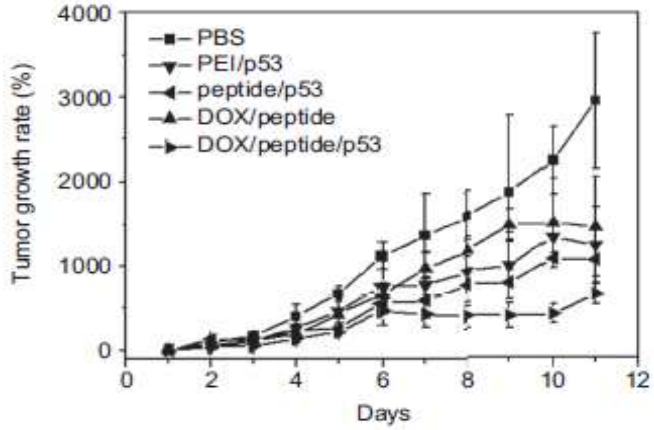

Fig. 11 *Anti-tumor effects after various treatments on H22 xenograft mice. Data are presented as mean ± S.D. (n = 6).*

The representative tumor imaging was shown in Fig. 12. Besides, the body weight of the group that injected with DOX/$(Fmoc)_2KH_7$-TAT/p53 DNA micelleplexes was relatively stable, suggesting the decreased side effect of this treatment by the use of peptide as well as the satisfactory anti-tumor effect, since the malignant growth of tumor increased the body weight to some extent.

Fig. 12 *imaging of the tumor at the 11th day after treatment of various formulations.*

10 ROS-triggered self-accelerating drug release nanosystem

Over the past decades, plenty of smart drug delivery systems (DDSs) have been proposed to overcome unwanted side effects and maximize therapeutic efficacy of tumor chemotherapy through achieving "on demand" drug release at tumor-targeted site under unique external or internal stimuli [25,26]. Besides the additional trigger of light and magnetic field, taking advantage of tumorrelated intrinsic stimuli, including overexpressed proteases, low pH value, hyperthermia and over secreted glutathione (GSH), stimuli-responsive DDSs could further mediate tumor microenvironment targeted therapy [27-32]. Recently, the relatively high level of intracellular reactive oxygen species (ROS) in tumor environment [33-35] was also exploited as a biochemical basis for researchers to propose innovative strategies for tumor-targeted treatment [36-38]. For example, Xia et al. developed a ROS sensitive cationic polymer (PATK) for targeted gene delivery. The containing thioketal cross-linkers could be cut away under abundant ROS environment, leading to the degradation of DNA/PATK polyplexes in PC3 cells, resulting in the release of DNA [39]. Although there are a variety of ROS cleavable bonds that have been utilized to endow the materials with ROS-responsibility, very few of them exhibit sufficient sensitivity to control the drug release efficiently at biological concentration of ROS, which is too low to trigger reaction *in vivo* [40].

To cope with the problem mentioned above, improving the sensitivity of materials might open up appealing possibilities. A good case in point is that Sung et al. reasonably utilized the H_2O_2 at biologically relevant concentration, which could diffuse into hollow microsphere carrier to generate CO_2 gas and disrupt the shell by reacting with a series of the encapsulated molecules, resulting in the release of loaded drug [41]. However, this strategy involved complicated design and syntheses. Besides constructing the ultrasensitive ROS-responsive carriers, another prevalent approach critically relies on the generated ROS during the processes of photodynamic therapy (PDT) to expand the utility of ROSresponsive reservoirs [42-45]. Nevertheless, precisely controlling of the irradiation time and intensity for extra laser source remains a hurdle. In addition, non-selectivity of ROS elevated in both normal cell and cancer cell under the irradiation scope could also cause lethal damage to healthy tissues.

Here, we proposed a ROS-triggered self-accelerating drug release nanosystem (defined as T/D@RSMSNs) based on a positive feedback strategy to overcome insufficient ROS generation of traditional DDSs through amplifying the intracellular ROS concentration, resulting in adequate drug release selectively in ROS abundant cancer cells in vivo. Firstly, as one of the most classic and primary nanocarriers, mesoporous silica nanoparticles (MSNs) were selected as drug carriers, owing to their distinct advantages, including large pore volume for loading drugs, easy surface functionalization and great biocompatibility [46-49]. Then, α-tocopheryl succinate (α-TOS), a vitamin E analogue, which could rapidly generate ROS in cells after interacting with mitochondrial respiratory complex II and interfering the electron transportation chain in mitochondria [50-52], and anticancer drug doxorubicin (DOX) were co-encapsulated in the pores of MSNs. The gatekeeper β-CD was anchored on the surface of MSNs through the ROS-cleavable thioketal linker (TK) for stimuli-responsive drug release [53]. Furthermore, adamantane conjugated poly(ethylene glycol) chain (AD-PEG) was introduced via host-guest interaction to enhance the stability of nanoparticles and prolong the circulation time *in vivo*. As shown in Scheme 3, after accumulation in tumor tissues through the enhanced permeability and retention (EPR) effect, T/D@RSMSN would be uptaken by tumor cell efficiently. At very beginning, only limited pores were open because of the existent but insufficient intracellular ROS, resulting in the simultaneous release of loaded DOX and α-TOS. Then, released α-TOS interacted with mitochondria in tumor cells to generate additional ROS. In other words, the intracellular ROS would be self-regenerated and amplified, which in turn facilitated the cutting of TK linkage to remove the gatekeeper β-CD and led to more release of α-TOS as well as DOX in MSNs.

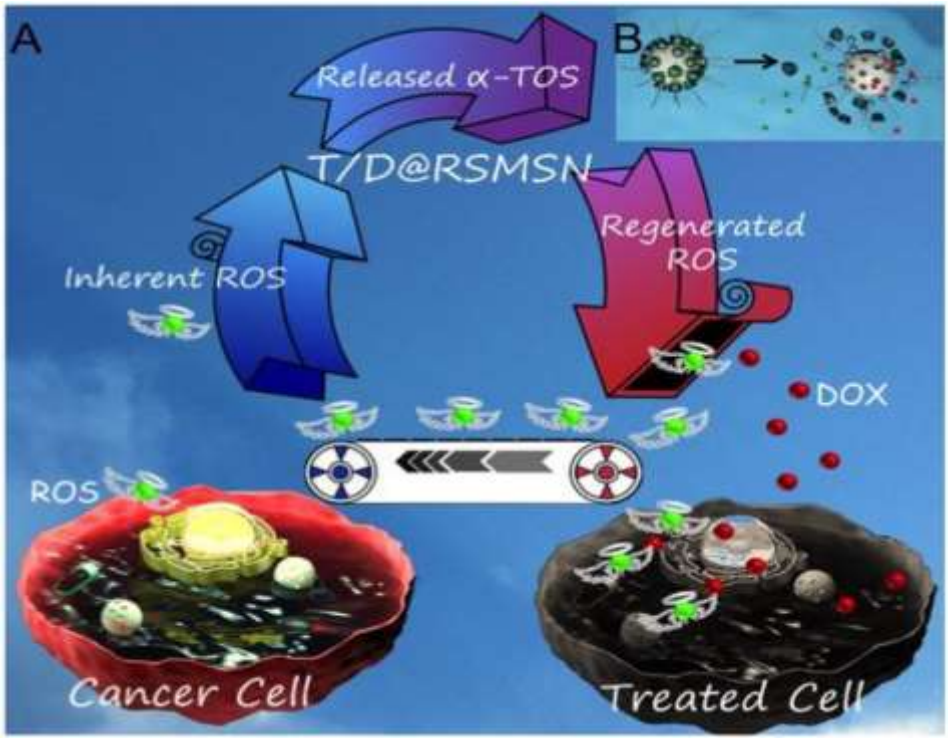

Scheme 3 *(A) Schematic representation of ROS-triggered self-accelerating drug release nanosystem for enhanced chemotherapy. After accumulation in tumor tissues through EPR effect, T/D@RSMSN was uptaken by tumor cell efficiently. Initially, only limited pores were open by the stimulating of inherent ROS, resulting in the release of restricted DOX and α-TOS. Owing to the ROS producing agent α-TOS, the intracellular ROS was self-regenerated, which could be regarded as new trigger and in turn facilitate the procedure of cutting away the TK, leading to more α-TOS and the self-accelerating release of toxic DOX. (B) Schematic structure of T/D@RSMSN.*

The detailed positive feedback effect with ROS-triggered self-accelerating drug release of this nanosystem was illustrated in Scheme 4. This novel nanosystem could not only achieve remarkable therapeutic effects, but also provide a general and vital strategy to surmount the restrictions of existing ROS-responsive DDSs.

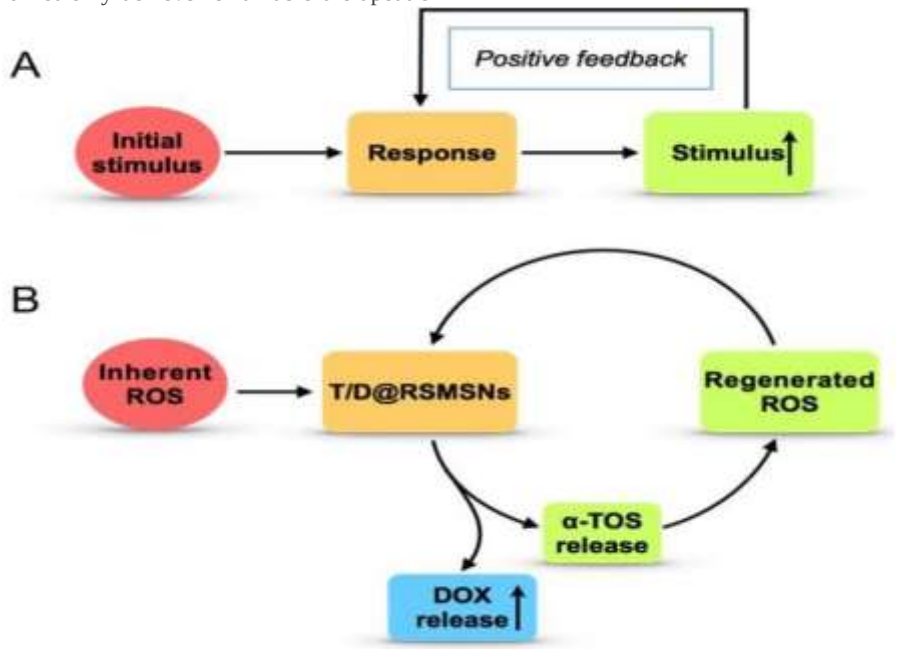

Scheme 4 *Schematic representation of (A) classical positive feedback loop (The response of initial stimulus could strengthen the stimulus) and (B) our ROS-triggered self-accelerating drug release nanosystem based on positive feedback strategy. After the stimulating of inherent ROS, the loaded α-TOS could be released from the pores of MSNs, which could interact with mitochondrion and produce regenerated ROS to reinforce this positive feedback loop. Along with positive circulation, the releasing of DOX could be accelerated.*

11 Characterization of T/D@RSMSNs

MSN was synthesized by using the classic basecatalyzed co-condensation methods with several modifications according to a previous report [54]. As shown in scanning electron microcopy (SEM) (Fig. 13A) and transmission electron microscopy (TEM) (Fig. 13B) images, well-distributed and uniform MSN with mesoporous structure and a mean diameter of ~65 nm was prepared successfully. The hydrodynamic diameter of MSN measured by dynamic light scattering (DLS) [55] was 116.1 nm (PDI = 0.029) and relatively larger than TEM size because of the hydrated layer surrounding the nanoparticles. The step-by-step functionalization on the surface of MSNs was monitored by zeta potential measurements (Fig.13C) and Fourier transforms infrared (FT-IR) spectra. As demonstrated in [55], the MSN was firstly reacted with 3-aminopropyltrimethoxysilane (APTMS) to obtain MSN-NH_2. After the surface modification of amino groups, the zeta potential of MSN-NH2 increased significantly from negatively charge of MSN (-17.73 mV) to positively charge (23.36 mV). Then the surfactant template (CTAC) in the pores of MSN was removed completely, and which was confirmed by the disappearance of characteristic absorption peak of CeH stretching vibrations at 2926 and 2854 cm^{-1} in FT-IR spectra. Subsequently, the ROScleavable thioketal linker (TK) [55] was introduced to the surface of MSN-NH_2 based on amide condensation reaction, giving rise to the negatively charged MSN-TK nanoparticles (-14.13 mV). DOX and a-TOS were co-loaded into the pores of MSNs after stirring the mixture solution of MSN-TK nanoparticles, DOX and α-TOS vigorously. Finally, the resultant nanoparticle was modified with the gatekeeper β-CD through another amide condensation reaction and long-circulating AD-PEG5000 was further introduced via host-guest interaction to obtain T/D@MSN-TK-CD/AD-PEG5000 (defined as T/D@RSMSN). As shown in Fig. 13D, in comparison with the distinct mesoporous structure of blank MSN, the mesostructure of T/D@RSMSN nanoparticles in TEM image was unclear and fuzzy after the cargoes loading and surface modification. In addition, the hydrodynamic diameter of MSNs measured by dynamic light scattering (DLS) increased with the continuous modification [55]. And the hydrodynamic diameter of T/D@RSMSN (Fig. 13E) was 159.2 nm (PDI = 0.110) with a monodisperse distribution, which was suitable for achieving the passive targeting to tumor tissue through EPR effect. To further explore the stability of nanosystems, hydrodynamic diameter changes of T/D@RSMSN in PBS and PBS with 10% serum after incubation for 24 h were measured. As indicated in [55], there was no significant aggregation during 24 h incubation, demonstrating well stability of T/D@RSMSN under physiological condition. Furthermore, thermogravimetric analysis (TGA) was employed to detect the weight loss of the nanoparticles after the stepwise decoration. As illustrated in Fig. 13F, when raising their temperature to 800 ºC, the weight loss of MSN-NH2, MSN-TK and T/D@RSMSN were 11%, 20% and 35%, respectively, which further confirmed the successful functionalization. Moreover, the mean number of CD molecules per nanoparticle was calculated to be 530 and the number of AD-PEG_{5000} conjugated on T/D@RSMSN could be calculated to be 431, according to the calculation method in a previous report [56]. Besides, as measured by the RF-5301PC spectrofluorophotometer and high performance liquid chromatography (HPLC), the loading efficiency (LE) of T/D@RSMSN was 5.1% for DOX and 2.5% for α-TOS. As to the control material D@MSNTK-CD/AD-PEG_{5000} (D@RSMSN), which only encapsulated DOX, the LE was 6.7%.

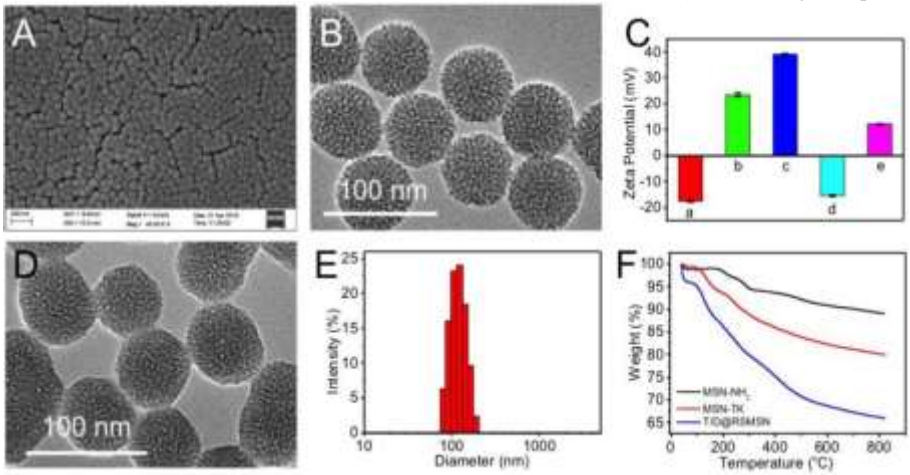

Fig. 13 Characterization of T/D@RSMSN. (A) SEM image of blank MSN. (B) TEM image of blank MSN. (C) Zeta potentials of (a) CTAC@MSN, (b) CTAC@MSN-NH2, (c) MSN-NH2, (d) MSN-TK, (e) T/D@RSMSN. (D) TEM image of T/D@RSMSN. (E) Hydrodynamic diameter of T/D@RSMSN measured by DLS analysis. (F) TGA curves of MSN-NH2, MSN-TK and T/D@RSMSN.

12 Evaluation of ROS responsive drug release

In this study, the T/D@RSMSN was capped by b-CD/AD through the ROS-cleavable TK linkers. After stimulating of ROS, the TK linkers would be broken, leading to the release of the loaded drug from the pores of nanoparticles. To investigate the ROS responsibility of this nanosystem, H_2O_2 was used as a typically ROS stimulus in in vitro experiments [42, 57], and the release profiles of the encapsulated DOX from T/D@RSMSN in PBS with different H_2O_2 concentration were monitored by spectrofluorophotometer. As shown in Fig. 14, without adding extra H_2O_2, T/D@RSMSN was gated by β-CD/AD effectively and less than 20% of drug was leaked even after 72 h incubation, proving the efficiency of anchoring of nanovalves through the TK linkers. In contrast, 60% DOX was released after the incubation with 100 μM H_2O_2 for 108 h. And when the nanoparticles were incubated with 1 mM H_2O_2, the release percentage of DOX reached 83% over 108 h. Apparently, the concentration of H_2O_2 had a remarkable and positive influence on the release rate and cumulative release amount of DOX, which was the basement of our self-accelerating drug release in cellular environments. Moreover, the release amount of a-TOS from T/D@RSMSN after incubating with different concentrations of H_2O_2 for 24 h was monitored by HPLC. As shown in [55], after incubating with different concentrations of H_2O_2 for 24 h, the accumulative release amount of α-TOS from T/D@RSMSN was enhanced markedly with the increased concentration of H_2O_2, confirming the successful ROS-responsible release of α-TOS, which was the prerequisite for ROS generation. The results above demonstrated that the β-CD/AD could act as an effective nanovalve and open the pores after the stimulating of ROS expectedly.

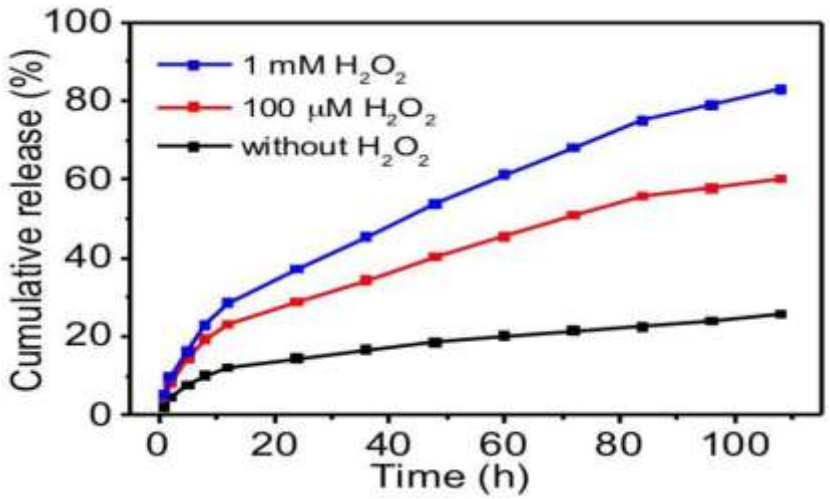

Fig. 14 *The drug release profiles of T/D@RSMSN incubated with different concentrations of H_2O_2.*

13 Analysis of the ROS regenerating ability of α-TOS in vitro

First of all, in order to better explore the feasibility of positive feedback strategy to overcome the obstacles in ROS-responsive DDSs, the frequently used ROS abundant human breast cancer cells (MCF-7) were chosen. And the prevailing intracellular ROS sensitive probe 2′,7-dichlorofluoresceindiacetate (DCFH-DA) was utilized to confirm the ROS generation. Cell permeable nonfluorescent DCFH-DA could be rapidly oxidized to dichlorofluorescein (DCF) with green fluorescence by the intracellular ROS [58]. As shown in Fig. 15A$_1$ and B$_1$, the conspicuous green fluorescence of DCF in MCF-7 cells clearly proved the inherently existence of intracellular ROS. Further, compared to the MCF-7 cells without staining (control), the fluorescence signal in MCF-7 cells incubated with DCFH-DA increased approximately 10 folds measured by the corresponding flow cytometry analysis (Fig. 15C).

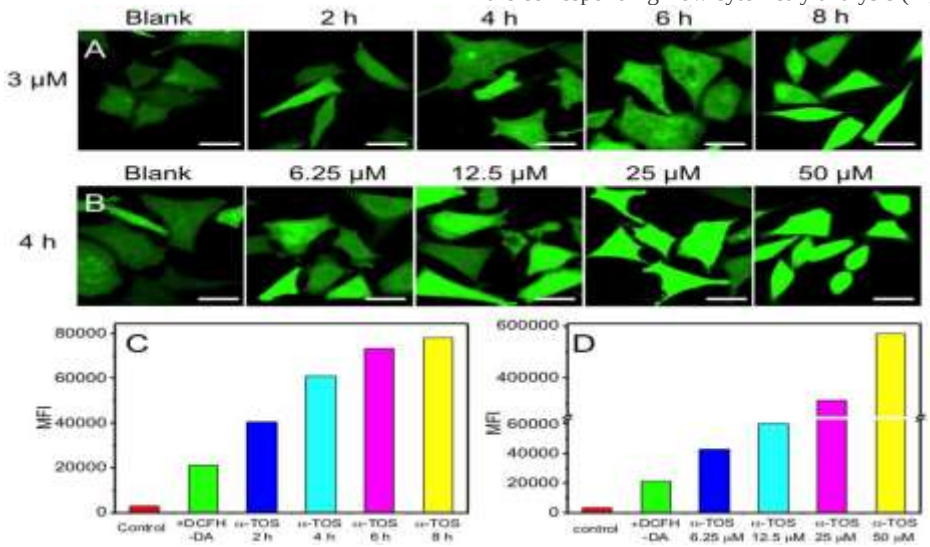

Fig. 15 *Evaluation of the ROS regenerating ability of α-TOS in vitro. CLSM images of MCF-7 cells treated with (A1-A5) 3 μM α-TOS for different time and (B1-B5) different concentration of α-TOS for 4 h. Green channel: DCF fluorescenceillustrated intracellular ROS. Scale bar: 20 μm. Quantitative analysis of MCF-7 cells treated with (C) 3 μM α-TOS for different time and (D) different concentration of α-TOS for 4 h by flow cytometry*

Afterwards, since the ROS generation of α-TOS was the key point in this positive feedback strategy based DDS, the intracellular ROS augmentation capability of α-TOS was also evaluated by the same ROS sensitive probe through confocal laser scanning microscopy (CLSM) and flow cytometry analysis. As shown in Fig. 15A and B, when the MCF-7 cells were incubated with α-TOS, the green fluorescent signal was noticeably stronger than that without α-TOS (blank), owing to the ROS generating capability of α-TOS, which could restrain the bioactivity of mitochondrial respiratory complex II, resulting in the electron transfer to produce ROS from oxygen. In addition, after prolonging the incubation time, the green fluorescence in MCF-7 cells incubated with a specific concentration of α-TOS (3 μM) became stronger (Fig. 15A). Besides the co-incubation time, the concentration of a-TOS is another factor to influence the levels of intracellular ROS. As demonstrated in Fig.15B, the fluorescent signal was enhanced markedly with the increased concentration of α-TOS. Thereafter, to quantitative investigate ROS producing ability of α-TOS, flow cytometry analysis was also conducted. As coincident with the CLSM results above, in the initial 2 h, the mean fluorescence intensity (MFI) values in MCF-7 cells increased to 1.5-fold, and up to 3.7-fold after prolonging the treated time to 8 h (Fig. 15C). Additionally, there was 2.8-fold and 26-fold increases of the levels of ROS in MCF-7 cells treated with 12.5 μM and 50 μM for 4 h, respectively

(Fig. 15D). Moreover, the ROS producing capability of α-TOS loaded in RSMSNs (T@RSMSNs) was also evaluated by CLSM. As shown in [55], with the increasing incubation time, the green fluorescence became stronger significantly, demonstrating the releasing of α-TOS from ROSresponsive nanocarriers. Further, no obviously change of green fluorescence indicated that the possible interfering of blank MSNs was excluded based on the same incubation conditions. These CLSM and flow cytometry analysis results above confirmed the intracellular ROS producing ability of α-TOS and also revealed the possibility of loading α-TOS for positive feedback strategy based DDS.

14 Intracellular ROS-triggered amplifying ROS signals and self accelerating drug release

Encouraged by the satisfying ROS generating capability of α-TOS, cellular co-incubation experiments were further performed to estimate the intracellular ROS-triggered ROS signals amplification and self-accelerating drug release efficiency of T/D@RSMSN in vitro. To highlight the important positive feedback effect induced by ROS producing agent, a single-DOX loaded nanoparticle with same modification, which was designed to like a traditional ROSresponsible DDS, was employed as a control group (defined as D@RSMSN). As shown in Fig. 16B_1-B_4, green fluorescencewas found in the MCF-7 treated with D@RSMSN, due to inherent ROS in MCF-7 cells. Although the green fluorescence was continuously existent, no obviously change was observed, even with increasing the incubation time from 4 h to 36 h, demonstrating that without α-TOS, the intrinsic intracellular ROS was barely growing. In addition, the red fluorescence of DOX, which was released from the pores of D@RSMSN after being uptaken, was clearly detected, but not enhanced significantly after prolonging the incubation time (Fig. 16C_1- C_4). It was understandable that as a result of limited intrinsic ROS, only a part of TK linkers of D@RSMSN could be cut away, leading to the partial release of DOX within the time allotted.

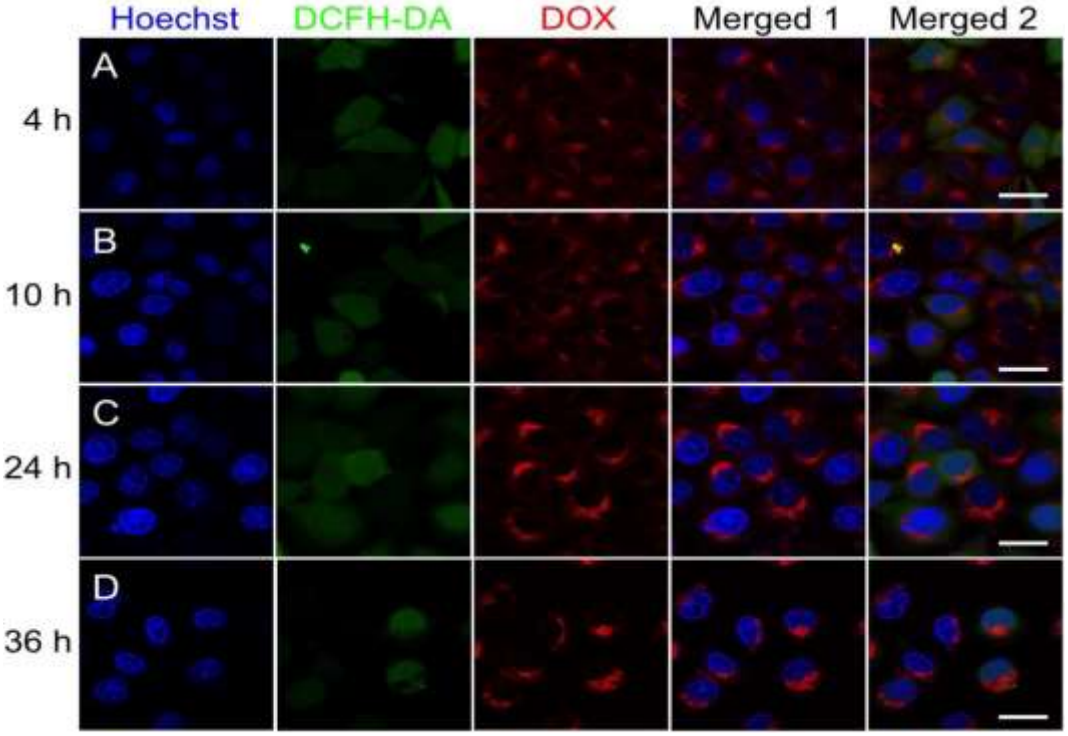

Fig. 16 *CLSM images of MCF-7 cells treated with control group D@RSMSN (CDOX: 2.5 μg/mL) for different time, respectively. Blue channel: Hoechst 33342 stained nucleus. Red channel: DOX. Green channel: DCF fluorescence illustrated intracellular ROS. Scale bar: 20 μm.*

Compared to the unsatisfying drug release situation of control group, the T/D@RSMSN nanoparticles have shown the high efficiency of ROS-triggered ROS signals amplification and selfaccelerating drug release *in vitro*. As illustrated in Fig. 17B_1- B_4, the green fluorescence was stronger than that in MCF-7 cells incubated with D@RSMSN (Fig. 17B_1-B_4) at each time point, indicating that besides the inherent intracellular ROS, the α-TOS also took effect on producing ROS. And with increasing incubation time, the green fluorescence was markedly increased, confirming that with the initial intracellular ROS triggering, the encapsulated α-TOS was released from the pores of T/D@RSMSN after the TK linkers were cleaved, resulting in the ROS regeneration and replenishment. What's more, augmenting levels of intracellular ROS would in turn assist in cutting away more TK linkers and produce the positive feedback effect. As expected, during this ROS triggered ROS amplification process, the co-loaded drug DOX showed a selfaccelerating release situation, which was proved by significantly increasing of red fluorescence signal with the extension of incubation time (Fig. 17C_1-C_4). Moreover, compared to the relatively weak red fluorescence in MCF-7 cells treated with D@RSMSN was mainly located in cytoplasm after incubating for 36 h, MCF-7 cells treated with T/D@RSMSN exhibited the strong red fluorescence in cytoplasm at 4 h and 10 h, stronger red fluorescence in cytoplasm and weak fluorescence in the nucleoplasm at 24 h, and after 36 h incubation, the red fluorescence of the released DOX spread throughout the whole MCF-7 cells (Fig. 17E). Further, quantitative fluorescence-intensity analysis by ImageJ software of red fluorescence (DOX) in MCF-7 cells showed that the released DOX amplified by α-TOS after incubation for 36 h was 1.9-fold higher than initial released DOX. These CLSM results demonstrated that the high efficiency of drug release in T/D@RSMSN based on ROS triggered positive feedback effect could improve the discontenting efficacy of omnipresent ROS-responsible DDS.

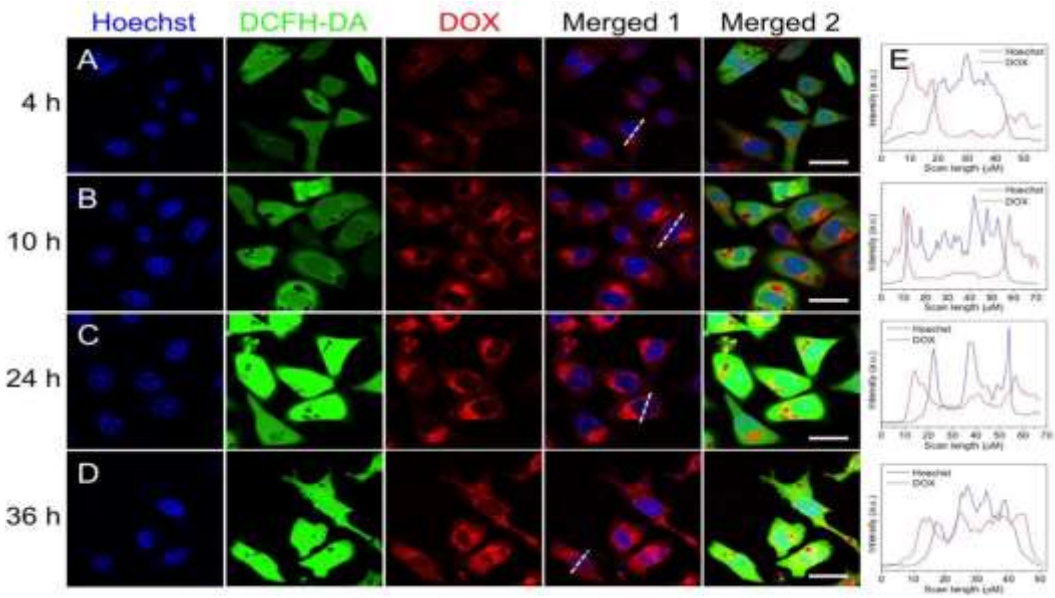

Fig. 17 (*AeD) CLSM images of MCF-7 cells treated with T/D@RSMSN (CDOX: 2.5 μg/mL) for different time, respectively. Blue channel: Hoechst 33342 stained nucleus. Red channel: DOX. Green channel: DCF fluorescence illustrated intracellular ROS. Scale bar: 20 μm. (E) Fluorescence signals based on the white line.*

To further evaluate the ROS microenvironment selective ability of T/D@RSMSN, human embryonic kidney (293T) normal cells with relatively negligible ROS were utilized as a control group. As shown in Fig. 18, compared to the obviously fluorescence in MCF-7 cells incubated with T/D@RSMSN or D@RSMSN, both negligible green fluorescence and red fluorescence were detected in 293T cells incubated with T/D@RSMSN or D@RSMSN, illustrating that without the abundant intracellular ROS, the pores were still capped and the loaded α-TOS and DOX could avoid being premature released from the nanoparticles, which was coincident with the cargoes release profiles above (Fig. 3). These results further confirmed that owing to the ROS cleavable TK linkers, the T/D@RSMSN could target to the tumor cells with high levels of ROS selectively, without affecting the healthy cells.

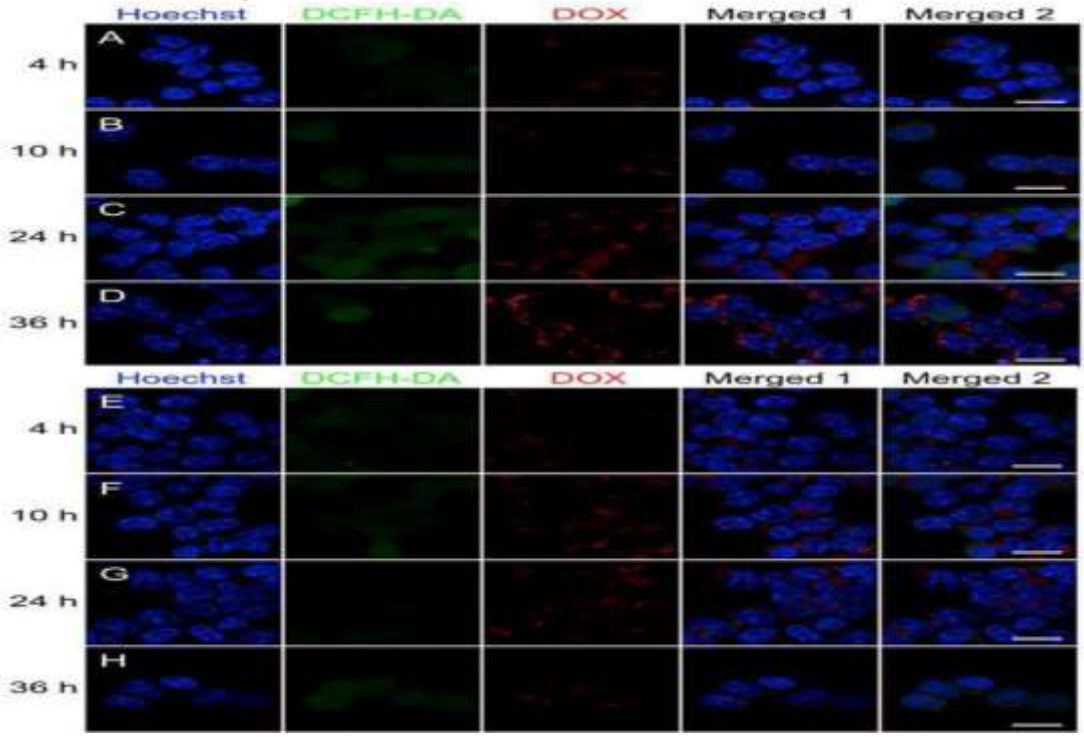

Fig. 18 *CLSM images of 293T normal cells treated with T/D@RSMSN (AeD) and D@RSMSN (EeH) (CDOX: 2.5 μg/mL) for different time, respectively. Blue channel: Hoechst 33342 stained nucleus. Red channel: DOX. Green channel: DCF fluorescence illustrated intracellular ROS. Scale bar: 20 μm.*

15 Evaluation of cytotoxicity in vitro of MSN

To testify the advantages of the ROS-triggered self-accelerating drug release nanosystem, the cell viability of MCF-7 cells and 293T cells treated with T/D@RSMSN and D@RSMSN was investigated. Firstly, the cytotoxicity of blank MSNs was evaluated. The cell viability of blank MSN in two cells was higher than 90%, even up to 100 μg/mL (Fig. 19), exhibiting low toxicity and suitability for drug delivery. Then, the cell viability of T/D@RSMSN or D@RSMSN in 293T cells had no obvious difference and was higher than 80% (Fig. 19A_1 and B_1), due to the nanoparticles were capped tightly without drug leakage under the really low concentration of ROS in normal cells. In comparison, the obviously cell viability was both observed in the MCF-7 cells incubated with T/D@RSMSN and D@RSMSN (Fig. 19A_1). Compared to the cell viability in 293T cells, the toxicity in MCF-7 cells was noticeable, because the gatekeepers of nanoparticles could be removed after being uptaken by tumor cells with relatively high levels of ROS, leading to the diffusion of DOX. Also, therewas a significant difference in cell toxicity between MCF-7 cells incubated with T/D@RSMSN and D@RSMSN. The cell viability of D@RSMSN in MCF-7 cells was 69%, due to the limited DOX release caused by nonsufficient ROS during the incubation time. In comparison with MCF-7 cells treated with D@RSMSN, the cell viability of T/D@RSMSN in MCF-7 cells was much lower (29%), because after the inherent ROS triggering, the intracellular ROS was regenerated by the released part of α-TOS, utilized as new triggers to release much more DOX during the incubation period, which was well matched with above CLSM results (Fig. 19A_2 and B_2). IC_{50} value (half inhibitory concentration) of T/D@RSMSN was 0.84 mg/L (DOX concentration), whichwas much lower than D@RSMSN (>2.5 mg/L) for MCF-7 cells, indicating advantages of positive feedback strategy of T/D@RSMSN. And the IC_{50} of free DOX was calculated to be 0.71 mg/L for MCF-7 cells and 0.76 mg/L for 293T cells. Furthermore, the cell viability of 293T cells or MCF-7 cells incubated with free α-TOS (Fig. 19A_4 and B_4) was supplied for reference. Therefore, this designed nanosystem could deliver the drug targeting to the ROS abundant tumor cells and produce the cell toxicity selectively, particularly achieve enhanced chemotherapy compared to the traditional ROS-responsive nanocarriers.

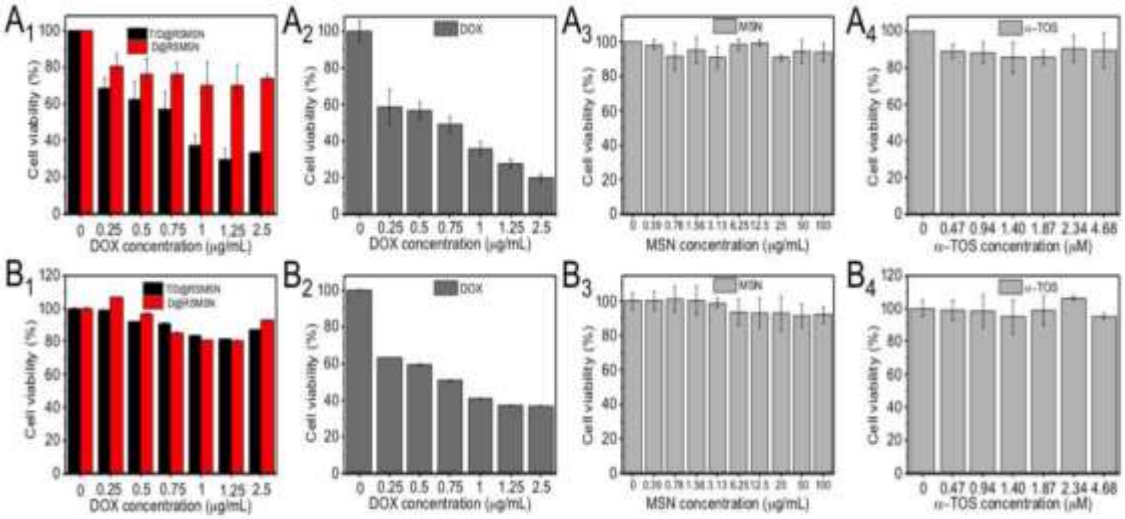

Fig. 19 *Cell viability of MCF-7 cells (A1-A4) and 293T cells (B1-B4) after being incubated with T/D@RSMSN and D@RSMSN (A1, B1), free DOX (A2, B2), blank MSN (A3, B3) and free α-TOS (A4, B4) for 48 h.*

16 Antitumor experiments in vivo via intravenous injection

Encouraged by the well performance in in vitro study, the feasibility of T/D@RSMSN in antitumor study in vivo was further evaluated through intravenous injection. The MCF-7 tumor-bearing nude mice were divided into four groups randomly (n > 5) and treated with PBS, free DOX, D@RSMSN and T/D@RSMSN, respectively. No obvious body weight variation was found in T/D@RSMSN group, confirming its well biocompatibility and nontoxicity (Fig. 20). The continuous tumor changes of MCF-7 tumor-bearing mice in each group during the 14 days treatment were exhibited through the digital photos (Fig. 20A). The tumor growth in the group injected with T/D@RSMSN was noticeably inhibited, in contrast with the other three groups. As displayed in Fig. 20C, the tumor volume in PBS group increased rapidly and grew to 10-fold of the initial volume after 14 days treatment. Moreover, the tumor treated with D@RSMSN could be inhibited to some extent, owing to the partial release of DOX triggered by the intracellular ROS. Compared to the free DOX, the main material T/D@RSMSN could inhibit the growth of tumor significantly, which illustrated the superiority of T/D@RSMSN in maximizing the antitumor efficiency, caused by positive feedback strategy. When all the mice were sacrificed after 14 days treatment, the tumors in each group were collected, average tumor weights (Fig. 20D) and the representative tumor photos (Fig. 20E) were provided to further confirm the therapeutic efficacy of T/D@RSMSN. Moreover, the therapeutic mechanism of T/D@RSMSN was studied by the terminal deoxynucleoitidyltransferaseddUTP nick end labeling (TUNEL) assay (Fig. 20F). An obvious large area of green fluorescence was displayed in T/D@RSMSN group, in comparison with none or a weak green fluorescent signal in other control groups, which was attributed to the cytotoxicity of the released DOX, leading to more apoptotic cells. In addition, hematoxylin and eosin (H&E) staining of tumor tissues was employed to evaluate the morphology and confirm the therapeutic efficiency of T/D@RSMSN. As exhibited in Fig. 20G, compared to abundant and compact tumor cells in PBS group and partial destroyed tumor cells in D@RSMSN or DOX group, the tumor cells in T/D@RSMSN group displayed that a more serious damage and many tumor cells were dead. These H&E staining and TUNEL staining assays results were coincident with the in vivo data of antitumor study above. Additionally, the low systemic toxicity of T/D@RSMSN was proved by no obviously pathological abnormalities in the heart, liver, spleen, lung, and kidney [55]. Furthermore, the normal myocardial five-enzyme parameters of the mice after treatment with T/D@RSMSN confirmed the T/D@RSMSN had no obvious cardiotoxicity [55]. These results above indicated that T/D@RSMSN displayed no systemic side effects and showed great potential in biomedical applications.

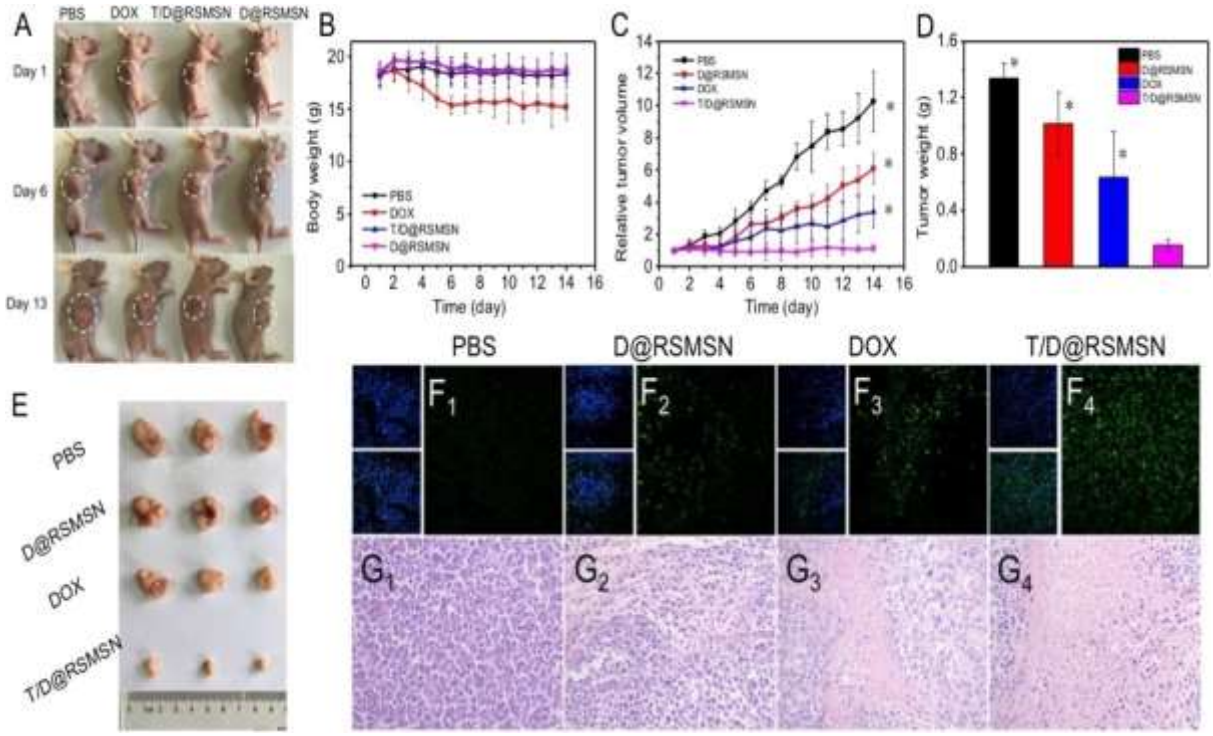

Fig. 20 *Antitumor experiments in vivo via intravenous injection. (A) Digital photos of MCF-7 tumor-bearing mice treated with PBS, free DOX, D@RSMSN and T/D@RSMSN during the 14 days evaluation period. (B) The body weight and (C) relative tumor volume of mice after different treatments. (D) Average tumor weight at the 14th day for each group. *p < 0.05 was analyzed by a Student's t-test when the group compared with T/D@RSMSN, respectively. (E) Photographs of tumor tissues at the 14th day after different treatments. (F) TUNEL immunofluorescence staining and (G) H&E staining images of tumors tissues, which were sacrificed at the 14th day. H&E staining: 200x magnification.*

17 Platinum-based combination chemotherapeutic drugs

Multiple randomized controlled trials during the last two decades have established combination chemotherapy (cisplatin-based) to be the standard of care as first-line treatment in recurrent or metastatic NSCLC [59,60]. Despite these advances, response rates to first-line platinum based therapy is approximately 30%, with median survival between 24 to 31 months [61]. Those who develop resistance to cisplatin receive pemetrexed, docetaxel, or erlotinib in the second-line setting, but response rates are only 7% to 10%. Improving our ability to manage the disease by optimizing the use of existing drugs and/or developing new agents is essential in this endeavor [62]. To this end, individualizing treatments by identifying patients who will or will not respond to specific agents will potentially increase the overall effectiveness of these drugs and limit the incidence and severity of toxicities that impair the functional status of patients and their ability to tolerate further therapies.

Standard treatment for advanced non–small-cell lung cancer (NSCLC) includes the use of a platinum-based chemotherapy regimen. However, response rates are highly variable. Newer agents, such as pemetrexed, have shown significant activity as second-line therapy and are currently being evaluated in the front-line setting. It has been utilized a genomic strategy [62] to develop signatures predictive of chemotherapeutic response to both cisplatin and pemetrexed to provide a rational approach to effective individualized medicine. Using in vitro drug sensitivity data, coupled with microarray data, it has been developed gene expression signatures predicting sensitivity to cisplatin and pemetrexed. Signatures were validated with response data from 32 independent ovarian and lung cancer cell lines as well as 59 samples from patients previously treated with cisplatin.

Since the advent of chemotherapy to treat cancer, there have been numerous advances in the development, selection, and application of these agents, sometimes with remarkable successes. In several instances, particularly in early-stage disease, combination chemotherapy in the adjuvant setting has been found to be curative. However, most patients with clinically or pathologically advanced solid tumors will eventually relapse and die as a result of their disease. For example, in advanced non–small-cell lung cancer (NSCLC), third-generation regimens consisting of a platinum analog in combination with a second agent increases overall response and survival when compared with older regimens [59,63,64]. However, overall response is still only 20% to 30%, [64] suggesting that a majority of the patients do not respond to a platinum analog. Subsequently, those patients who experience treatment failure with platinum-based therapy typically receive pemetrexed, docetaxel, or targeted therapies as secondline treatment, with response rates of approximately 7% to 10% [65-67].

New technologies offer the potential to measure genome-wide gene activity that may serve as a powerful adjunct to currently available clinical and biochemical markers. Such complementary approaches may better characterize the complexity of the disease and identify discrete clinical and biologically relevant phenotypes [68-70]. The ability to find structure in the data, in the form of patterns of gene expression, provides snapshots of gene activity in a cell or tissue sample that can then be used to describe a phenotype [71, 72]. This transforms biology from an observational molecular science to a data-intensive quantitative genomic science [73-75]. The dimension and complexity of such data provide an opportunity to uncover patterns and trends that can distinguish subtle phenotypes in ways that traditional methods cannot.

Recently, we have described the use of gene expression profiling to develop signatures of drug sensitivity to individual chemotherapeutic

drugs [76]. These signatures also reliably predicted in vitro and in vivo response to individual cytotoxic drugs. Thus, development of gene expression profiles that can predict response to commonly used cytotoxic agents may provide a unique opportunity to better utilize drugs previously shown to be effective in first- or second-line therapy. Here, we describe a novel approach to rationalized drug therapy in NSCLC, by developing predictors of cisplatin (a first-line agent) and pemetrexed (a second-line agent) sensitivity and demonstrating the clinical value of identifying the most appropriate drug on the basis of sensitivity profile for the treatment regimen of each individual patient, thus moving beyond empirical therapeutic choices that are now in current practice. Such an approach is likely to maximize response to chemotherapeutic drugs and may change the current paradigm of cancer therapy, particularly in NSCLC, and possibly in other advanced cancers.

17.1 Cell and RNA preparation

Full details of the methods used for RNA extraction and development of gene expression data from lung and ovarian tumors have been described previously [70, 76].

Briefly, total RNA was extracted using the Qiashredder and Qiagen RNeasy Mini kit (Qiagen, Hilden, Germany) and the quality of RNA was checked by an Agilent 2100 Bioanalyzer (Agilent Technologies, Palo Alto, CA). The targets for Affymetrix DNA microarray analysis were prepared according to the manufacturer's instructions. Biotin-labeled cRNA, produced by in vitro transcription, was fragmented and hybridized to the Affymetrix U133A Gene- Chip arrays at 45°C for 16 hours and then washed and stained using the GeneChip Fluidics (Affymetrix). The arrays were scanned by a GeneArray Scanner (Affymetrix) and patterns of hybridization were detected as light emitted from the fluorescent reporter groups incorporated into the target and hybridized to oligonucleotide probes. All analyses [62] were performed in a MIAME (minimal information about a microarray experiment)-compliant fashion, as defined in the guidelines established by Microarray Gene Expression Data (MGED).

17.2 Classification of platinum response in ovarian tumors

Using Affymetrix U133A GeneChips, it has been measured [62] gene expression in 59 patients with advanced (International Federation of Gynecology and Obstetrics stage III/IV) serous epithelial ovarian carcinomas who received cisplatin therapy (Gene Expression Omnibus [GEO] accession number: GSE3149). All ovarian cancer specimens were obtained at initial cytoreductive surgery from patients and collected under the respective (Duke University Medical Center, Durham, NC, and H. Lee Moffitt Cancer Center, Tampa, FL) institutional review board protocols involving written informed consent.

Response to therapy was evaluated using standard criteria for patients with measurable disease, based on WHO guidelines [77]. CA-125 was used to classify responses only in the absence of a measurable lesion and based on established guidelines [78]. A complete response (CR) was defined as a complete disappearance of all measurable and assessable disease or, in the absence of measurable lesions, a normalization of the CA-125 level after salvage therapy. A partial response (PR) was considered a 50% or greater reduction in the product obtained from measurement of each bidimensional lesion for at least 4 weeks or a drop in the CA-125 by at least 50%for at least 4 weeks. Progressive disease (PD) was defined as a 50% or greater increase in the product from any lesion documented within 8 weeks of initiation of therapy, appearance of any new lesion within 8 weeks of initiation of therapy, or a doubling of CA-125 from baseline. For the purposes of our analysis, a clinically beneficial response (ie, "responder") included CRor PR.Apatient who did not demonstrate aCR or PR was considered a "nonresponder."

17.3 Cross-Platform affymetrix Gene Chip Comparison

To map the probe sets across various generations of Affymetrix Gene-Chip arrays, we utilized Chip Comparer (http://tenero.duhs.duke.edu/genearray/perl/chip/chipcomparer.pl) as described previously [70,76].

17.4 Cell Proliferation and Drug Sensitivity Assays

Optimal cell number and linear range of drug concentration were determined [62] for each cell line and drug as described previously [70, 76]. For drug sensitivity assay, cells were plated in non–drug-containing media in 96-well plates. After incubation for 24 hours at 37°C, drugs were added to each well at a specific concentration. Cells were grown in the presence of drugs for an additional 96 hours, and sensitivity to cisplatin, docetaxel, paclitaxel, and pemetrexed in the cell lines was determined by quantifying the percent reduction in growth (*v* dimethyl sulfoxide [DMSO] controls) at 96 hours using a standard MTT colorimetric assay (CellTiter 96 Aqueous One 23 Solution Cell Proliferation Assay Kit; Promega, Madison, WI) [79, 80].

18 Developing a gene expression–based predictor of cisplatin sensitivity

The experimental strategy for analysis employed in that study [62] is similar to that used for the development of oncogenic pathway and chemotherapy sensitivity signatures as described previously [70,76]. Samples representing extreme cases are used to train the expression data to develop a genomic signature that can predict drug sensitivity. A predictor of cisplatin sensitivity was developed by analyzing cell lines described by Györffy et al [81].

Using Bayesian binary regression analysis, genes highly correlated with drug sensitivity were identified and used to develop a model that could differentiate between cisplatin sensitivity and resistance. The developed model consisting of 45 genes based on cisplatin sensitivity (Fig. 21A) was validated in a leave-one-out cross-validation. The cisplatin sensitivity predictor includes DNA repair genes such as *ERCC1* and *ERCC4*, among others, that had altered expression in the list of cisplatin sensitivity predictor genes. Interestingly, one previously described mechanism of resistance to cisplatin therapy results from the increased capacity of cancer cells to repair DNA damage incurred, by activation of DNA repair genes [82, 83].

18.1 Developing a gene expression–based predictor of pemetrexed sensitivity

In NSCLC, where platinum-based therapy is the standard of care, response rates are only 30%. One approach to identifying potential drugs effective in cisplatin-resistant patients is to examine the NCI-60 data set for agents whose IC_{50} profile showed an inverse relationship with cisplatin, focusing on those known to be effective in NSCLC. Of these drugs, an inverse correlation with cisplatin sensitivity was identified with docetaxel, abraxane, and pemetrexed. The strongest inverse correlation was found between cisplatin and pemetrexed sensitivity ($P<.001$; Pearson r value, 0.1; $\alpha = 0.05$).

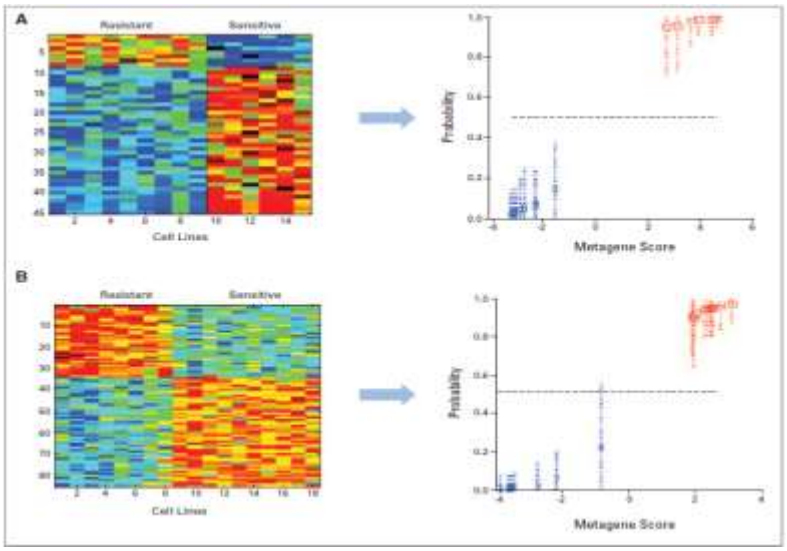

Fig. 21 *(A) Cisplatin and (B) pemetrexed sensitivity predictor. Left panels show the expression plot for genes discriminating the cisplatin or pemetrexed sensitive and resistant cell lines. Each column represents individual cell lines and each row individual genes in the predictors. Right panels show the accuracy in a leave-one-out cross-validation.Blue, low probability of drug sensitivity; red, high probability of drug sensitivity.*

Using methods previously described [76], a predictor of pemetrexed sensitivity was developed by identifying NCI-60 cell lines that were most resistant or sensitive to pemetrexed. Using Bayesian binary regression analysis, genes whose expression was most highly correlated with drug sensitivity were used to develop a predictive model that could differentiate between pemetrexed sensitivity and resistance. The developed model consisting of 85 genes based on pemetrexed sensitivity (Fig. 21B) was validated in a leave-one-out cross-validation. Interestingly, multiple genes involved in nucleotide and cellular metabolism constituted the pemetrexed sensitivity predictor and is biologically consistent with the known mechanism of pemetrexed sensitivity, which involves interference with cell-cycle progression by reducing the pool of substrates necessary for DNA replication [84].

19 In Vitro validation of the cisplatin and pemetrexed predictor

In addition to initial leave-one-out cross-validation, the true value of a predictor lies in its ability to predict sensitivity in independent in vitro and in vivo settings. In the present study [62], the predictor of cisplatin sensitivity was independently validated in a panel of 32 (lung and ovarian cancer) cell lines, using cell proliferation assays and concurrent gene expression data. As shown in Figure 22A, the correlation between the predicted probability of sensitivity to cisplatin (in both lung and ovarian cell lines) and the respective IC_{50} for cisplatin confirmed the capacity of the cisplatin predictor to accurately predict sensitivity to the drug in cancer cell lines.

Similar to the independent validation of the cisplatin sensitivity predictor, the pemetrexed predictor was validated using gene expression data from an independent cohort of 17 NSCLC cell lines with respective in vitro drug sensitivity assays. As shown in Figure 22B, the correlation between the predicted probability of sensitivity to pemetrexed in the 17 NSCLC cell lines and the respective IC_{50} for pemetrexed validated the ability of the pemetrexed predictor to predict sensitivity to the drug in an independent cohort of cancer cell lines.

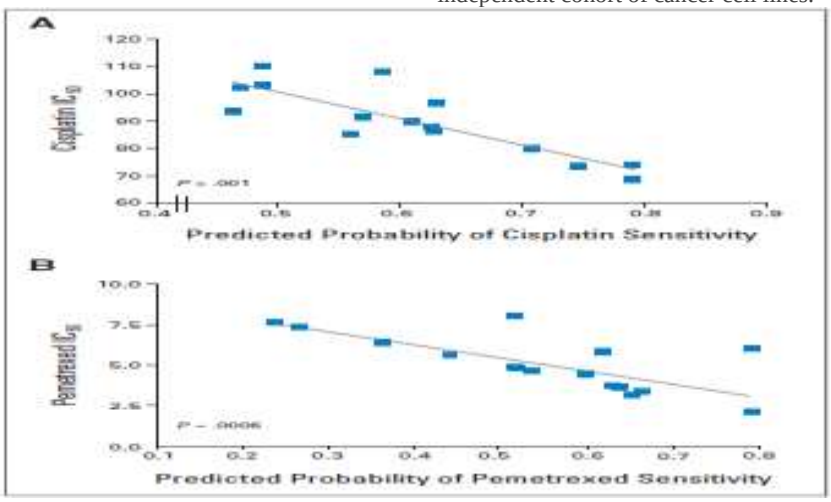

Fig. 22 *In vitro validation of the cisplatin and pemetrexed predictors. (A) Fifty percent inhibitory concentration (IC50) of cisplatin plotted against predicted sensitivity to cisplatin in cell lines predicts sensitivity to the drug (P < .001 [top, ovarian] and P = .03 [bottom, lung]). (B) IC50 of pemetrexed plotted against the predicted probability to pemetrexed predicts sensitivity to pemetrexed in non– small-cell lung cancer lines (P = .0006).*

19.1 In Vivo validation of the cisplatin sensitivity Predictor

Although the ability of the cisplatin signature to predict sensitivity in independent samples validates the performance of the signature, it is the ability to predict response in patients that is obviously most critical. Using data from a previously published study that linked gene expression data with clinical response to cisplatin in an ovarian data set [70] (GEO accession number: GSE3149), it has been tested the ability of the in vitro cisplatin sensitivity predictor to accurately identify those patients who experience disease response with cisplatin. Using a predicted probability of response of 0.50 as the cutoff for predicting cisplatin sensitivity, the accuracy of the in vitro gene expression–based predictor of cisplatin sensitivity, based on available clinical data, was 83.1% (sensitivity, 100%; specificity, 57%; positive predictive value [PPV], 78%; negative predictive value [NPV], 100%; Fig.23). Furthermore, a Mann-Whitney*U*test revealed a significant difference in the predicted probabilities of cisplatin sensitivity between the resistant and sensitive cohorts of patients (*P*<.01; Fig. 23).

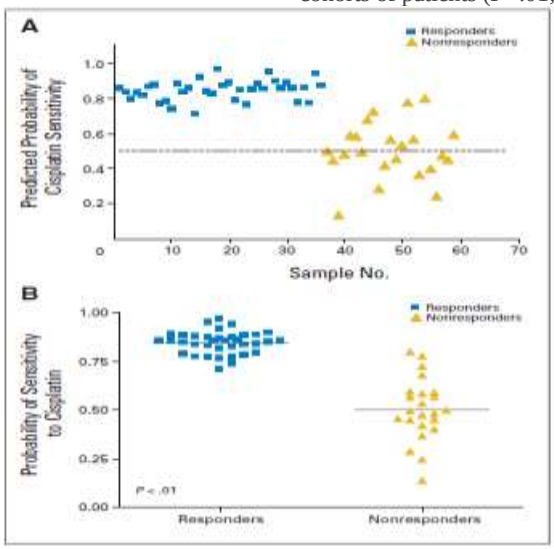

Fig. 23 *In vivo validation of cisplatin sensitivity predictor. Part (A) represents the predicted probability of cisplatin sensitivity in patients classified as responders and nonresponders. Part (B) is a single-variable scatter plot of a significance test of the predicted probabilities of sensitivity to cisplatin in the same samples (Mann-Whitney U test P < .01).*

20 Patterns of predicted chemotherapy response to cisplatin and pemetrexed in NSCLC

The cisplatin and pemetrexed predictors were utilized to profile the potential options of using these two drugs in a collection of 91 NSCLC described previously [85] (GEO accession number: GSE3141). These samples were first sorted according to the patterns of predicted sensitivity to cisplatin (Fig. 24A, left panel). The pattern observed indicated that those patients resistant to cisplatin (red) weremoresensitive to pemetrexed (blue). Although the data points in the scatter plot do not appear to be perfectly correlated, this analysis suggests that the relationship was statistically significant (*P* = .004, log-rank; Fig. 24A, right panel). A similar relationship was also demonstrated in the independent cohort of NSCLC cell lines (Fig.24B), suggesting the possibility of an alternative therapy for treatment of advanced or metastatic NSCLC patients who would be predicted to be platinum resistant. As a comparison, the pemetrexed signature was also applied to the ovarian cancer patient data set. In this analysis [62], however, only two (< 4%) of 59 patients were identified to have greater than 50% probability of being sensitive to pemetrexed.

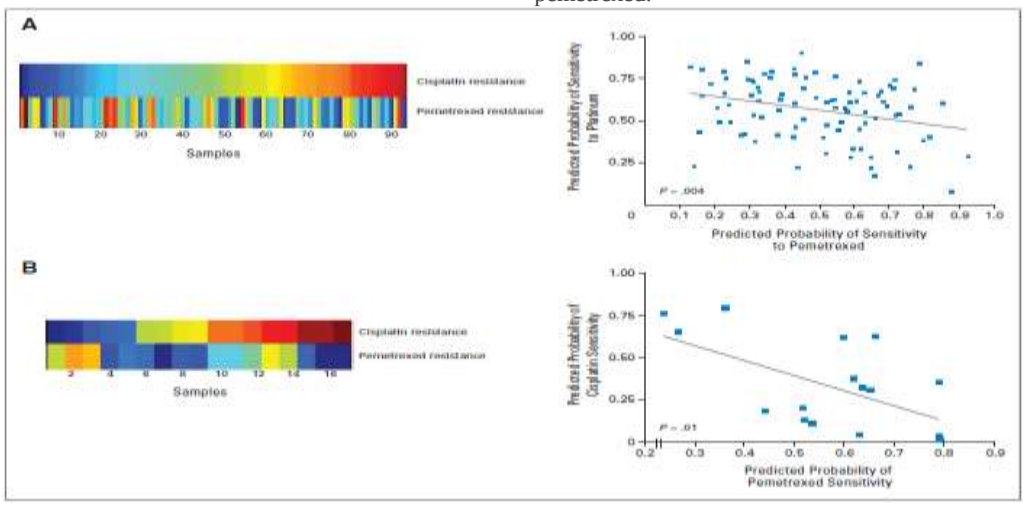

Fig. 24 *Correlation between cisplatin and pemetrexed sensitivity in (A) lung tumors and (B) cell lines. Top row represents the probability of cisplatin resistance and bottom row the corresponding probability of pemetrexed resistance for each sample. Right panels show the inverse relationship between predicted cisplatin and pemetrexed resistance (P = .004) and cell lines (P = .01).*

21 The sequence of chemotherapy may be critical in optimizing responses

Currently, first-line treatment with a platinum-based regimen is the standard of care for advanced NSCLC. Those patients developing resistance to cisplatin are treated with a taxane, pemetrexed, or erlotinib as second-line options. To explore the effect of cisplatin resistance, as well as prior treatment with potentially ineffective therapies, the IC_{50} of various lung cancer cell lines to cisplatin and pemetrexed were analyzed and revealed an inverse relationship (Fig. 25A). Thereafter, one NSCLC cell line (H2030) that is resistant to cisplatin, paclitaxel, and docetaxel, but sensitive to pemetrexed on the basis of cell proliferation assays (IC_{50}), was treated with pemetrexed, docetaxel, or paclitaxel in a systematic fashion. Interestingly, when H2030 was first treated for 4days with a taxane (docetaxel or paclitaxel), resistance to subsequent pemetrexed exposure was induced (Fig. 25B). In contrast, when H2030 was first treated with pemetrexed, H2030 was sensitive, as expected (Fig. 25B). Although these in vitro observations are only hypothesis generating at this time, this proof of principle experiment [62] suggests that the sequence of second-line chemotherapy in NSCLCmayprove to be important in determining clinical outcomes. Specifically, in tumors from cisplatin-refractory patients who are also predicted to be resistant to a taxane, treatment with a taxane (docetaxel or paclitaxel) before pemetrexed therapy may induce resistance to subsequent pemetrexed therapy. This preliminary observation, pending further validation, suggests the importance of including genomic-based, disease-specific, treatment prioritization in clinical practice.

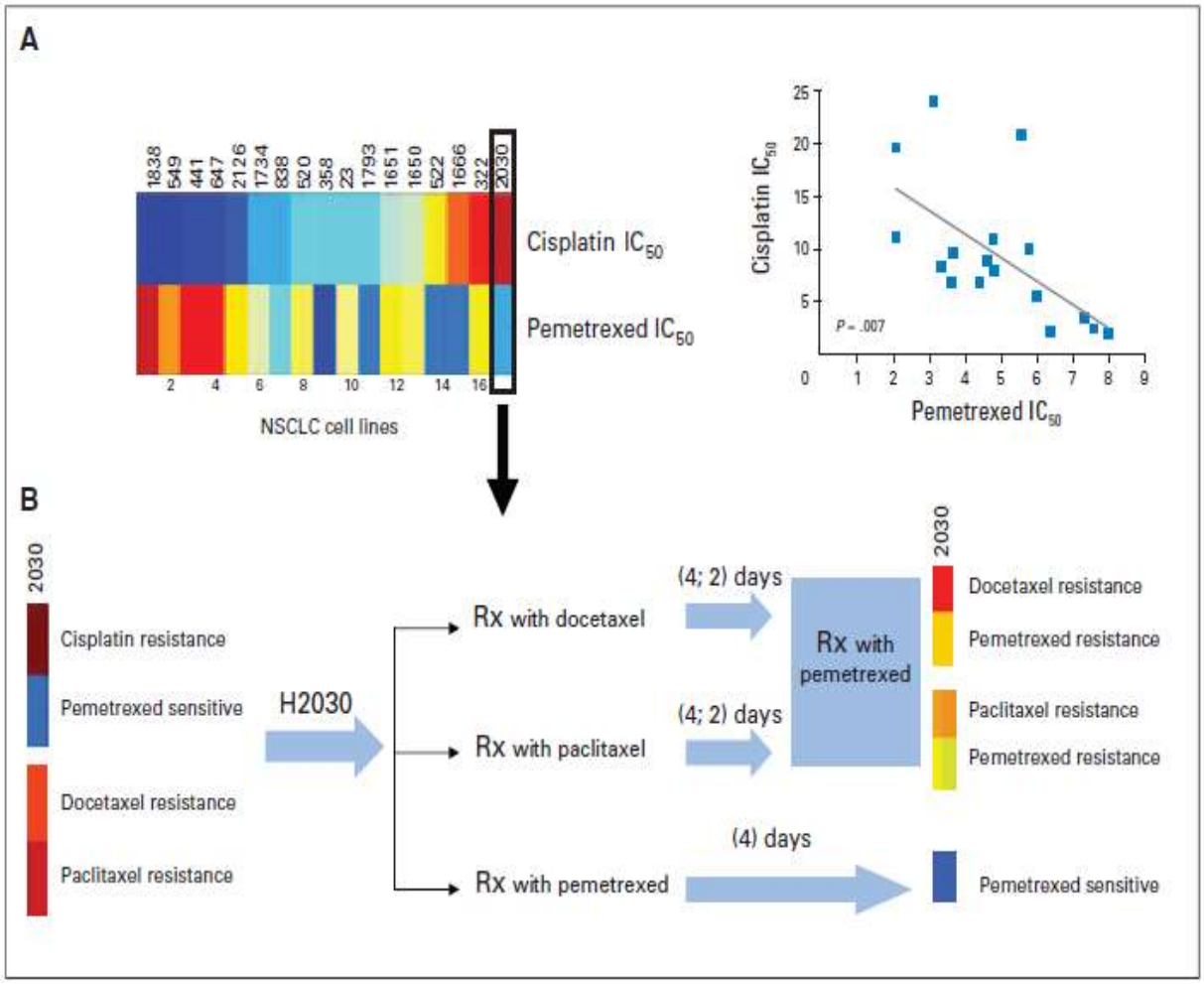

Fig. 25 *Sequence of chemotherapy may be critical in optimizing responses. (A) Fifty percent inhibitory concentration (IC50) of lung cancer cell lines to cisplatin and pemetrexed reveal a significant inverse relationship. (B) The non–small-cell lung cancer (NSCLC) cell line (H2030) is initially pemetrexed sensitive. After exposure to a taxane for 4 days, H2030 subsequently develops resistance to pemetrexed. Rx, treatment drug.*

In this study [62], the patterns of cisplatin sensitivity observed in our cohort of 91 NSCLC tumors suggests that not all patients may initially respond to first-line cisplatin-based therapy. As described herein, response rates to first-line platinum based therapy is approximately 30%, with median survival between 24 to 31 months [61].We have made use of in vitro drug sensitivity data in cancer cell lines, coupled with Affymetrix expression data, to develop gene expression signatures reflecting sensitivity to cisplatin and pemetrexed. The capacity of these signatures to predict response in independent sets of cell lines and patient studies begins to define a strategy that addresses the potential to identify cytotoxic agents that best match individual patients with advanced NSCLC and other advanced cancers (ovarian cancer). In addition, it can potentially be applied to patients with early-stage NSCLC to predict who may benefit from adjuvant cisplatin-based therapy. However, as promising as these approaches may seem, these strategies need to be first validated in a prospective clinical trial that would evaluate the performance of a genomic signature-based selection as an initial step in the individualized treatment strategy for patients with advanced NSCLC (Fig. 26).

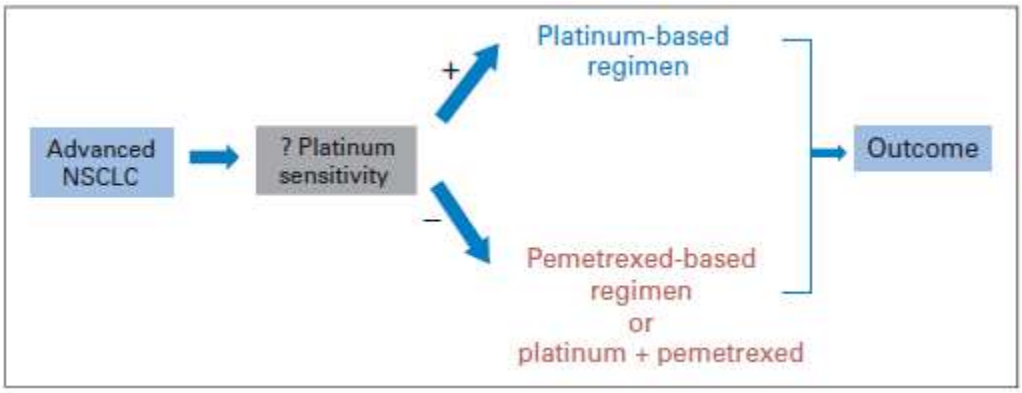

Fig. 26 *An example of a possible future treatment strategy for patients with advanced non–small-cell lung cancer (NSCLC). +, sensitive to cisplatin; -, resistant to cisplatin.*

In conclusion, the development of signatures of drug sensitivity provide an opportunity to optimize therapy for patients with NSCLC and perhaps other patients with advanced cancer where cisplatinbased therapy is considered the standard of care.

22 Conclusions

In this review, an amphiphilic chimeric peptide $(Fmoc)_2KH_7$-TAT was designed and synthesized. $(Fmoc)_2KH_7$-TAT peptide possessed good capacity of loading DNA and DOX simultaneously. The existence of H_7 sequence in $(Fmoc)_2KH_7$-TAT peptide led to a much higher DOX release rate from$(Fmoc)_2KH_7$-TAT peptide at pH 5.0 than that at pH 7.4. At the same time, H7 sequence endowed the peptide/DNA complexes with well endosome escaping ability. $(Fmoc)_2KH_7$-TAT peptide mediated excellent transfection efficacy both in 293T and HeLa cell-lines under serum-free and serum-containing conditions. Besides, $(Fmoc)_2KH_7$-TAT micelle exhibited much superiority in transporting gene and drug to the same cells simultaneously and exhibited satisfactory synergistic effect both in vitro and in vivo. The results demonstrated a promising peptide-based micelle nanoplatform for efficient delivery [86-89] of gene and drug simultaneously and synergistic therapy in the realm of tumor treatment.

In summary, a novel ROS-triggered self-accelerating drug release nanosystem by amplifying the intracellular ROS concentration based on the positive feedback strategy was designed for enhanced tumor chemotherapy. It was found that owing to the ROS cleavable TK linkers, this designed nanosystem could deliver the drug to the ROS abundant tumor cells and produce the cell toxicity selectively, without affecting the normal cells. Moreover, both in vitro and in vivo studies proved that in MCF-7 cells, T/D@RSMSNs could not only release DOX and a-TOS initiatively, but also lead to the augmented concentration of intracellular ROS by α-TOS and accelerating release of DOX, displaying more remarkably antitumor activity than the traditional ROS-responsive nanocarriers. This novel ROS-triggered self-accelerating drug release nanosystem with enhanced tumor therapeutic efficiency could provide a general strategy to branch out the applications of existing ROSresponsible DDSs.

References

1. Kai Han, Si Chen, Wei-Hai Chen (2013) Synergistic gene and drug tumor therapy using a chimeric peptide. *Biomaterials* 34 4680-4689.
2. Jones B (2012) Tumor genetics: evaluating oncogene cooperativities. *Nat Rev Genet*; 13:598.
3. Chi DS, Musa F, Dao F, Zivanovic O, Sonoda Y, Barakat RR, et al (2012) An analysis of patients with bulky advanced stage ovarian, tubal, and peritoneal carcinoma treated with primary debulking surgery (PDS) during an identical time period as the randomized EORTC-NCIC trial of PDS vs neoadjuvant chemotherapy (NACT). *Gynecol Oncol* 124:10-4.
4. Bock C, Lengauer T (2012) Managing drug resistance in tumor: lessons from HIV therapy. *Nat Rev Cancer* 12:494-501.
5. Sun TM, Du JZ, Yao YD, Mao CQ, Dou S, Wang J, et al (2011) Simultaneous delivery of siRNA and paclitaxel via a "two-in-one" micelleplex promotes synergistic tumor suppression. *ACS Nano* 5:1483-94.
6. MacDiarmid JA, Amaro-Mugridge NB, Madrid-Weiss J, Sedliarou I, Wetzel S, Brahmbhatt H, et al (2009) Sequential treatment of drug-resistant tumors with targeted minicells containing siRNA or a cytotoxic drug. Nat Biotechnol 27:643-51.
7. Han L, Huang RQ, Li JF, Liu SH, Huang SX, Jiang C (2011) Plasmid pORF-hTRAIL and doxorubicin co-delivery targeting to tumor using peptide-conjugated polyamidoamine dendrimer. *Biomaterials* 32:1242-52.
8. Wang HJ, Zhao PQ, Su WY, Wang S, Liao ZY, Chang J, et al (2010) PLGA/polymeric liposome for targeted drug and gene co-delivery. *Biomaterials* 31: 8741-8.
9. Liu SH, Guo YB, Huang RQ, Li JF, Huang SX, Jiang C (2012) Gene and doxorubicin co-delivery system for targeting therapy of glioma. *Biomaterials* 33: 4907-16.
10. Lu X, Wang QQ, Xu FJ, Tang GP, Yang WT (2011)A cationic prodrug/therapeutic gene nanocomplex for the synergistic treatment of tumors. *Biomaterials* 32: 4849-56.
11. Meng H, Liong M, Xia T, Li ZX, Ji ZX, Nel AE, et al (2010) Engineered design of mesoporous silica nanoparticles to deliver doxorubicin and P-glycoprotein siRNA to overcome drug resistance in a tumor cell line. *ACS Nano* 4: 4539-50.
12. Lv HT, Zhang SB, Wang B, Cui SH, Yan J (2006) Toxicity of cationic lipids and cationic polymers in gene delivery. *J Control Release* 114:100-9.
13. Pack DW, Hoffman AS, Pun S, Stayton PS (2005) Design and development of polymers for gene delivery. *Nat Rev Drug Discov* 4:581-93.
14. Nakase I, Kobayashi S, Futaki S (2010) Endosome-disruptive peptides for improving cytosolic delivery of endosome-disruptive peptide. *Biopolymers* 94: 763-70.
15. Wang Y, Gao SJ, Ye WH, Yoon HS, Yang YY (2006) Co-delivery of drugs and DNA from cationic coreeshell nanoparticles self-assembled from a biodegradable copolymer. *Nat Mater* 5:791-6.
16. Xiong XB, Lavasanifar A (2011) Traceable multifunctional micellar nanocarriers for tumor-targeted co-delivery of MDR-1 siRNA and doxorubicin. *ACS Nano* 5:5202-13.
17. Alexis F, Lo SL, Wang S (2006) Covalent attachment of low molecular weight poly (ethyleneimine) improves Tat peptide mediated gene delivery. Adv Mater 18:2174-8.

18. Hoyer J, Neundorf I (2012) Peptide vectors for the nonviral delivery of nucleic acids. *Acc Chem Res* 45:1048-56.
19. Seth P, Willingham MC, Pastan I (1985) Binding of adenovirus and its external proteins to Triton X-114. *J Biol Chem* 260:14431-4.
20. Kakudo T, Chaki S, Futaki S, Nakase I, Akaji K, Harashima H, et al (2004) Transferrinmodified liposomes equipped with a pH-sensitive fusogenic peptide: an artificial viral-like delivery system. *Biochemistry* 43:5618-28.
21. Kichler A, Leborgne C, Marz J, Danos O, Bechinger B (2003) Histidine-rich amphipathic peptide antibiotics promote efficient delivery of DNA into mammalian cells. *Proc Natl Acad Sci U S A* 100:1564-8.
22. Yi WJ, Yang J, Li C, Wang HY, Zhuo RX, Zhang XZ, et al (2012) Enhanced nuclear import and transfection efficiency of TAT peptide based gene delivery systems modified by additional nuclear localization signals. *Bioconjug Chem* 23:125-34.
23. Han K, Yang J, Chen S, Chen CJ, Zhuo RX, Zhang XZ, et al (2012) Novel gene transfer vectors based on artificial recombinant multi-functional oligopeptides. *Int J Pharm* 436:555-63.
24. Lu DX, Wen XT, Liang J, Gu ZW, Zhang XD, Fan YU (2009) A pH-sensitive nano drug delivery system derived from pullulan/Doxorubicin conjugate. J Biomed Mater Res B 89B:177-83.
25. S. Mura, J. Nicolas, P (2013) Couvreur, Stimuli-responsive nanocarriers for drug delivery, Nat. Mater. 12 991-1003.
26. J. Du, L.A. Lane, S. (2015) Nie, Stimuli-responsive nanoparticles for targeting the tumor microenvironment, *J. Control. Release* 219 205-214.
27. J.J. Hu, L.H. Liu, Z.Y. Li, R.X. Zhuo, X.Z (2016) Zhang, MMP-responsive theranostic nanoplatform based on mesoporous silica nanoparticles for tumor imaging and targeted drug delivery, *J. Mater. Chem.* B 4 1932-1940.
28. J. Zhang, Z.F. Yuan, Y (2013) Wang, W.H. Chen, G.F. Luo, S.X. Cheng, et al., Multifunctional envelope-type mesoporous silica nanoparticles for tumor-triggered targeting drug delivery, *J. Am. Chem*. Soc. 135 5068-5073.
29. H.J. Li, J.Z. Du, X.J. Du, C.F. Xu, C.Y. Sun, H.X. Wang, et al., (2016) Stimuli-responsive clustered nanoparticles for improved tumor penetration and therapeutic efficacy, Proc. Natl. Acad. Sci. U.S.A. 113 4164-4169.
30. 30K. Han, W.Y. Zhang, J. Zhang, Q. Lei, S.B. Wang, J.W. Liu, et al., (2016) Acidity-triggered tumor-targeted chimeric peptide for enhanced intra-nuclear photodynamic therapy, Adv. *Funct.Mater*. 26 4351-4361.
31. D.W. Zheng, J.L. Chen, J.Y. Zhu, L. Rong, B. Li, Q. Lei, et al., (2016) Highly integrated nano-platform for breaking the barrier between chemotherapy and immunotherapy, Nano Lett.16 4341-4347.
32. J.J. Hu, D. Xiao, X.Z. Zhang, (2016) Advances in peptide functionalization on mesoporous silica nanoparticles for controlled drug release, Small 12 3344-3359.
33. D. Trachootham, J. Alexandre, P. (2009) Huang, Targeting cancer cells by ROSmediated mechanisms: a radical therapeutic approach? Nat. Rev. Drug Discov. 8 579-591.
34. Y. Kuang, K. Balakrishnan, V. Gandhi, X. (2011) Peng, Hydrogen peroxide inducible DNA cross-linking agents: targeted anticancer prodrugs, J. Am. Chem. Soc. 133 19278-19281.
35. C.Tapeinos, A (2016) Pandit, Physical, chemical, and biological structures based on ROS-sensitive moieties that are able to respond to oxidative microenvironments, Adv. Mater. 28 5553-5585.
36. X. Liu, J. Xiang, D. Zhu, L. Jiang, Z. Zhou, J. Tang, et al., (2016) Fusogenic reactive oxygen species triggered charge-reversal vector for effective gene delivery, Adv. Mater. 28 1743-1752.
37. M. Wang, S. Sun, C.I. Neufeld, B.P. Ramirez, Q (2014) Xu, Reactive oxygen speciesresponsive protein modification and its intracellular delivery for targeted cancer therapy, Angew. Chem. Int. Ed. 53 13444-13448.
38. W.H. Chen, G.F. Luo, W.X. Qiu, Q (2016) Lei, S. Hong, S.B. Wang, et al., Programmed nanococktail for intracellular cascade reaction regulating self-synergistic tumor targeting therapy, Small 12 733-744.
39. M.S. Shim, Y (2013) Xia, A reactive oxygen species (ROS)-responsive polymer for safe, efficient, and targeted gene delivery in cancer cells, Angew. *Chem. Int.* Ed. 52 6926-6929.
40. C. de Gracia Lux, S. Joshi-Barr, T. Nguyen, E. Mahmoud, E. Schopf, N. Fomina, et al., (2012) Biocompatible polymeric nanoparticles degrade and release cargo in response to biologically relevant levels of hydrogen peroxide, *J. Am. Chem. Soc.* 134 15758-15764.
41. M.F. Chung, W.T. Chia, W.L. Wan, Y.J. (2015) Lin, H.W. Sung, Controlled release of an anti-inflammatory drug using an ultrasensitive ROS-responsive gas-generating carrier for localized inflammation inhibition, J. Am. Chem. Soc. 137 12462-12465.
42. K. Han, J.Y. Zhu, S.B. (2015) Wang, Z.H. Li, S.X. Cheng, X.Z. Zhang, Tumor targeted gold nanoparticles for FRET-based tumor imaging and light responsive on-demand drug release, *J. Mater. Chem*. B 3 8065-8069.
43. J. Lee, J. Park, K. Singha (2013) Mesoporous silica nanoparticle facilitated drug release through cascade photosensitizer activation and cleavage of singlet oxygen sensitive linker, Chem. Commun.1545-1547.
44. G. Yang, X. Sun, J. Liu, L. Feng, Z. (2016) Liu, Light-responsive, singlet oxygentriggered on-demand drug release from photosensitizer-doped mesoporous silica nanorods for cancer combination therapy, Adv. *Funct .Mater*. 264722-4732.
45. Y. Yuan, J. Liu, B. (2014) Liu, Conjugated-polyelectrolyte-based polyprodrug: targeted and image-guided photodynamic and chemotherapy with on-demand drug release upon irradiation with a single light source, *Angew. Chem. Int. Ed*. 53 7163-7168.
46. Q. He, J. Shi (2014) MSN Anti-cancer nanomedicines: chemotherapy enhancement, overcoming of drug resistance, and metastasis inhibition, Adv. Mater. 26 391-411.
47. Z. Li, J.C. Barnes, A. Bosoy, J.F. Stoddart, J.I. (2012) Zink, Mesoporous silica nanoparticles in biomedical applications, Chem. Soc. Rev. 41 2590e2605.
48. P. Yang, S. Gai, J. (2012) Lin, Functionalized mesoporous silica materials for controlled drug delivery, Chem. Soc. Rev. 41 3679-3698.
49. F. Tang, L. Li, D. (2012) Chen, Mesoporous silica nanoparticles: synthesis, biocompatibility and drug delivery, Adv. Mater. 24 1504-1534.
50. L.F. Dong, P. Low, J.C. Dyason, X.F. Wang, L. (2008) Prochazka, P.K. Witting, et al., a-Tocopheryl succinate induces apoptosis by targeting ubiquinone-binding sites in mitochondrial respiratory complex II, Oncogene 27 4324-4335.
51. M. Stapelberg, N. Gellert, E. Swettenham, M. Tomasetti, P.K. (2005) Witting, A. Procopio, et al., a-Tocopheryl succinate inhibits malignant mesothelioma by disrupting the fibroblast growth factor autocrine loop Mechanism and the role of oxidative stress, J. Biol. Chem. 280 25369-25376.
52. Y.H. Kang, E. Lee, M.K. Choi, J.L. Ku, S.H. Kim, Y.G. Park, et al., (2004) Role of reactive oxygen species in the induction of apoptosis by a-tocopheryl succinate, Int. J. Cancer 112 385-392.

53. D.S. Wilson, G. Dalmasso, L. (2010) Wang, S.V. Sitaraman, D. Merlin, N. Murthy, Orally delivered thioketal nanoparticles loaded with TNF-a-siRNA target inflammation and inhibit gene expression in the intestines, Nat. Mater. 9 923-928.
54. L. Pan, Q. He, J. Liu, Y. Chen, M. Ma, L. (2012) Zhang, et al., Nuclear-targeted drug delivery of TAT peptide-conjugated monodisperse mesoporous silica nanoparticles, *J. Am. Chem.* Soc. 134 5722-5725.
55. Jing-Jing Hu, Qi Lei, Meng-Yun Peng, Di-Wei Zheng,Yi-Xuan Chen, Xian-Zheng Zhang (2017) A positive feedback strategy for enhanced chemotherapy based on ROS-triggered self-accelerating drug release nanosystem. *Biomaterials* 128 136-146.
56. Q. Zhang, X. Wang, P.Z. Li, K.T. Nguyen, X.J (2014) Wang, Z. Luo, et al., Biocompatible, uniform, and redispersible mesoporous silica nanoparticles for cancertargeted drug delivery in vivo, Adv. *Funct. Mater*. 24 2450-2461.
57. H.L. Pu, W.L. Chiang, B. Maiti, Z.X. Liao, Y.C. Ho, M.S. Shim, et al (2014) Nanoparticles with dual responses to oxidative stress and reduced ph for drug release and anti-inflammatory applications, *ACS Nano* 8 1213-1221.
58. B. Genty, J. Briantais, N. Baker (1989) The relationship between the quantum yield of photosynthetic electron transport and quenching of chlorophyll fluorescence, Biochem. Biophys. Acta 990 87-92.
59. Bunn PA Jr (1998) Kelly K: New chemotherapeutic agents prolong survival and improve quality of life in non-small cell lung cancer: A review of the literature and future directions. *Clin Cancer Res* 4:1087-1100
60. Shepherd FA (1994) Treatment of advanced nonsmall cell lung cancer. *Semin Oncol* 21:7-18, (suppl)
61. Breathnach OS, Freidlin B, Conley B, et al (2001) Twenty-two years of phase III trials for patients with advanced non-small-cell lung cancer: Sobering results. *J Clin Oncol* 19:1734-1742.
62. David S. Hsu, Bala S. Balakumaran, Chaitanya R. Acharya, Vanja Vlahovic, Kelli S , (2010) Walters, Katherine Garman, Carey Anders, Richard F. Riedel, Johnathan Lancaster, David Harpole, Holly K. Dressman, Joseph R. Nevins, Phillip G. Febbo, and Anil Potti. Pharmacogenomic Strategies Provide a Rational Approach to the Treatment of Cisplatin-Resistant Patients with Advanced Cancer. JOURNAL OF CLINICAL ONCOLOGYVOLUME 25, NUMBER 28, OCTOBER 1 2007. This article was retracted on November 16.
63. Kelly K, Crowley J, Bunn PA, et al (2001) Randomized phase III trial of paclitaxel plus carboplatin versus vinorelbine plus cisplatin in the treatment of patients with advanced non-small cell lung cancer: A Southwest Oncology Group trial. *J Clin Oncol* 19: 3210-3218,
64. Schiller JH, Harrington D, Belani CP, et al (2002) Comparison of four chemotherapy regimens for advanced non-small cell lung cancer. *N Engl J Med* 346:92-98
65. Fossella FV, DeVore R, Kerr RN, et al (2000) Randomized Phase III trial of docetaxel versus vinorelbine or ifosamide in patients with non small cell lung cancer previously treated with platinum containing chemotherapy regiments. *J Clin Oncol* 18:2354-2362
66. Hanna N, Shepherd FA, Fossella FV, et al (2004) Randomized phase III trial of pemetrexed vs docetaxel in patients with NSCLC previously treated with chemotherapy. *J Clin Oncol* 22:1589-1597
67. Shepherd FA, Rodrigues Pereira J, Cieleanu T, et al (2005) Erlotinib in previously treated non small cell lung cancer. *N Engl J Med* 353:123-132
68. Golub TR, Slonim DK, Mesirov J, et al (1999) Molecular classification of cancer: Class discovery and class prediction by gene expression profiling. Science 286:531-537
69. Golub TR: Genome-wide views of cancer. N Engl J Med 344:601-602
70. Bild A, Yao G, Chang JT, et al (2006) Oncogenic pathways signatures in human cancers as guide to targeted therapies. Nature 439:353-357
71. Perou CM, Sorlie T, Eisen MB, et al (2000) Molecular portraits of human breast tumors. Nature 406:747-752
72. Rosenwald A, Wright G, Chan WC, et al (2002) The use of molecular profiling to predict survival after chemotherapy for diffuse large B cell lymphoma. N Engl J Med 346:1937-1947
73. Shipp MA, Ross KN, Tamayo P, et al (2002) Diffuse large B-cell lymphoma outcome prediction by geneexpression profiling and supervised machine learning. *Nat Med* 8:68-74
74. van de Vijver MJ, He YD, van't Veer LJ, et al (2002) A gene expression signature as a prediction of survival in breast cancer. *N Engl J Med* 347:1999-2009
75. Ramaswamy S, Ross KN, Lander ES, et al (2003) A molecular signature of metastasis in primary solid tumor. *Nat Genet* 33:49-54
76. Potti A, Dressman HK, Bild A, et al (2006) Genomic signatures to guide the use of chemotherapeutics. *Nat Med* 12:1294-1300
77. Therasse P, Arbuck SG, Eisenhauer EA, et al (2000) New guidelines to evaluate the response to treatment in solid tumors: European Organization for Research and Treatment of Cancer, National Cancer Institute of the US, National Cancer Institute of Canada. *J Natl Cancer Inst* 92:205-216
78. Rustin GJ, Timmers P, Nelstrop A, et al: (2006) Comparison of CA-125 and standard definitions of progression of ovarian cancer in the intergroup trial of cisplatin and paclitaxel versus cisplatin and cyclophosphamide. *J Clin Oncol* 24:45-51
79. Mosmann T: (1983) Rapid Colorimetric Assay for Cellular Growth and Survival: Application to proliferation and cytotoxic assay. *J Immunol Meth* 65:55-63
80. Berridge MV, Tan AS: (1993) Characterization of the cellular reduction of 3-(4,5-dimethylthiazol-2-yl)-2,5-diphenyltetrazolium bromide (MTT): Subcellular localization, substrate dependence, and involvement if mitochondrial electron transport in MTT reduction. *Arch Biochem Biophys* 303:474-482
81. Györffy B, Surowiak P, Kiesslich O, et al: (2006) Gene expression profiling of 30 cancer cell lines predicts resistance towards 11 anticancer drugs at clinically achieved concentrations. *Int J Cancer* 118:1699-1712
82. Johnson S, Perez R, Godwin A, et al: (1994) Role of platinum-DNA adduct formation and removal in cisplatin resistance in human ovarian cancer cell lines. *Biochem Pharmacol* 47:689-697
83. Yen L, Woo A, Christopoulopoulos G, et al: (1995) Enhanced host cell reactivation capacity and expression of DNA repair genes in human breast cancer cells resistant to bi-functional alkylating agents. *Mutat Res* 337:179-189
84. Paz-Ares, Bezares S, Tabernero J, et al: (2003) Review of a promising new agent in pemetrexed disodium. *Cancer* 97:2056-2063
85. Potti A, Mukherjee S, Petersen R, et al: (2006) A genomic strategy to refine prognosis in early-stage non–small-cell lung cancer. *N Engl J Med* 355:570-580
86. Loutfy H. Madkour Book: Reactive Oxygen Species (ROS), Nanoparticles, and Endoplasmic Reticulum (ER) Stress-Induced Cell Death Mechanisms. Paperback ISBN: 9780128224816
87. Loutfy H. Madkour Book : (2020) Nanoparticles Induce Oxidative and Endoplasmic Reticulum Antioxidant Therapeutic Defenses.Copyright *Publisher Springer International Publishing*
88. Loutfy H. Madkour Book: Nucleic Acids as Gene Anticancer Drug Delivery Therapy. 1st Edition .Publishing house:Elsevier, (2020). Paperback ISBN: 9780128197776 Imprint: Academic

Press Published Date: 2nd January 2020 Imprint: Academic Press Copyright: Paperback ISBN: 9780128197776 © Academic Press 2020 Published: 2nd January 2020 Imprint: Academic Press Paperback ISBN: 9780128197776

89. Loutfy H. Madkour Book: Nanoelectronic Materials: Fundamentals and Applications (Advanced Structured Materials) 1st ed. 2019 Edition: Series Title Advanced Structured Materials Series Volume 116 Copyright 2019 Publisher

DOI: 10.31579/IJBR-2021/035